Role of the Cys loop and transmembrane domain in the allosteric modulation of α4β2 nicotinic acetylcholine receptors

Constanza Alcaino[1], Maria Musgaard[2], Teresa Minguez[1], Simone Mazzaferro[1], Manuel Faundez[3], Patricio Iturriaga-Vasquez[4], Philip C Biggin[2] and Isabel Bermudez[1*]

[1]Department of Biological and Medical Sciences, Oxford Brookes University, Oxford OX3 0BP, United Kingdom. [2]Department of Biochemistry, University of Oxford, Oxford OX1 3QU, United Kingdom. [3]Faculty of Sciences, University of Chile, Santiago, Chile. [4]Departamento de Ciencias Quimicas y Recursos Naturales; Facultad de Ingenieria y Ciencias, Universidad de la Frontera, Temuco, Chile

Running title: Transduction pathways in α4β2 nicotinic receptor potentiation

To whom correspondence should be addressed: Isabel Bermudez, Department of Biological and Medical Sciences, Oxford Brookes University, Oxford OX3 0BP, U.K., Tel.: +44 1865 483146, FAX: +44 1865 483242, E-mail: ibermudez@brookes.ac.uk

Keywords: C-terminal, Cys loop, nicotinic acetylcholine receptors, positive allosteric modulators, pentameric ligand-gated ion channels, transduction pathway, transmembrane domain, post-M4.

ABSTRACT

Allosteric modulators of pentameric ligand gated ion channels (pLGICs) are thought to act on elements of the pathways that couple agonist binding to channel gating. Using α4β2 nicotinic acetylcholine receptors (nAChRs) and the α4β2-selective positive modulators 17β-estradiol (βEST) and desformylflustrabromine (dFBr), we have identified pathways that link the binding sites for these modulators to the Cys loop, a region that is critical for channel gating in all pLGICs. Previous studies have shown that the binding site for potentiating βEST is in the C-terminal (post-M4 region) of the α4 subunit. Here, using homology modelling in combination with mutagenesis and electrophysiology, we identified the binding site for potentiating dFBr on the top-half of a cavity between the third (M3) and fourth transmembrane (M4) α-helices of the α4 subunit. We found that the binding sites for βEST and dFBr communicate with the Cys loop, through interactions between the last residue of post-M4 and F170 of the conserved FPF sequence of the Cys loop, and that these interactions affect potentiating efficacy. In addition, interactions between a residue in M3 (Y309) and F167, a residue adjacent to the Cys loop FPF motif, also affect dFBr potentiating efficacy. Thus, the Cys loop acts as a key control element in the allosteric transduction pathway for potentiating βEST and dFBr. Overall, we propose that positive allosteric modulators that bind the M3-M4 cavity or post-M4 region increase the efficacy of channel gating through interactions with the Cys loop.

The α4β2 nicotinic acetylcholine receptor (nAChR) belongs to the superfamily of pentameric ligand gated ion channels (pLGICs). In humans, this superfamily comprises the Cys loop receptors (including muscle and neuronal nAChRs, 5-HT_3, $GABA_A$, and glycine receptors), which mediate all fast central nervous system synaptic inhibition and much of fast peripheral excitation. Cys loop receptor subunits assemble as a pentamer of identical (homomeric channels) or different (heteromeric channels) subunits around a central ion channel. The individual subunits have a large extracellular N terminal domain (ECD) that consists of 10 β-strands (β1-β10) folded into a β-sandwich, and a transmembrane domain (TMD) with four transmembrane α helices (M1 to M4) connected by linkers (M1-M2, M2-M3, M3-M4), as well as intracellular domains and a highly variable extracellular C-terminal (post-M4) region (1). There are 2-5 neurotransmitter binding sites at subunit interfaces within the ECD, and these are functionally coupled to the transmembrane ion channel located ca. 50 Å away. In the nAChR, the subunit contributing the principal face of the agonist binding site (an α subunit) couples agonist-triggered agonist binding site movements to channel gating (2, 3). The coupling is achieved at the ECD-TMD interface by a principal pathway that couples the pre-M1 region in the ECD to the M2-M3 linker through the β1-β2 loop (4) and the canonical FPF motif of the β6-β7 loop (the Cys loop) (5, 6). More recently, it has been shown that gating is also affected by more peripheral pathways that couple M4 to M1 and M3 (7) and, post-M4 to the Cys loop (8).

In common with all members of the pLGIC family, the current responses of α4β2 nAChR can be enhanced by a variety of agents, including Zn^{2+} (9, 10), the endogenous steroid 17β-estradiol (βEST) (11), desformylflustrabromine (dFBr) (12, 13) and synthetic ligands CMPI (14), LY2087101 (15), and NS206 and NS9283 (16, 17). The identification of positive allosteric modulator (PAM) binding sites in the TMD of the α4 subunit, e.g. βEST and NS206 binding sites (11, 17), as well as on the signature α4/α4 interface present in α4β2 nAChRs composed of three α4 and two β2 subunits (potentiating Zn^{2+}, CMPI and NS9283 binding sites) (10, 14, 17), has revealed the critical role of this subunit in sensitivity to PAMs. Despite this insight, there is little understanding of how PAM binding to sites in the α4 subunit is transduced into receptor potentiation. Allosteric modulators are thought to induce the same global conformational transitions that promote channel opening by agonists by affecting gating elements nearby their binding sites (18). In this respect, it is significant that the β1-β2 loop and Cys loop in the α4 subunit have been identified as components of the transduction pathway linked to potentiation of α4β2 nAChRs by the NS206 binding site in the TMD (17). Additionally, W621, the first residue in the N-terminal side of the post-M4 region of the α4 subunit, has been shown to affect βEST potentiating efficacy in a manner consistent with a role in transduction (19).

A suitable model system to examine the role of post-M4 and ECD agonist-binding-gating coupling elements in positive allostery of α4β2 nAChRs is that involving potentiation of this receptor type through PAM sites located in the α4 subunit. An example of this type of α4β2 nAChR PAM is βEST, whose binding site is in the post-M4 region of the α4 subunit (11). To identify additional allosteric modulator binding sites on the α4 subunit, we performed docking of nicotinic PAMs on a homology model of the α4β2 nAChR. These studies highlighted dFBr as a PAM that may bind the upper part of the TMD of the α4 subunit. By using mutagenesis together with the substituted cysteine accessibility method (SCAM), we confirmed that the upper half of a cavity between M3 and M4 hosts a potentiating dFBr site. Here, we demonstrate that allosteric signals from the dFBr and βEST potentiating binding sites are propagated to the Cys loop through interactions between F170 of the canonical FPF motif of the Cys loop and the final residue of the post-M4 region. We also found that interactions between F167 in the Cys loop and Y309 in M3 are also important for the transduction of dFBr binding into potentiation of the α4β2 nAChR.

RESULTS

The TMD of the α4 nAChR subunit houses a potentiating dFBr binding site. We examined the role of post-M4 and agonist binding-gating coupling elements in the α4 subunit in the propagation of allosteric signals generated by binding of the PAM compounds βEST and dFBr to α4β2 nAChRs. The potentiating efficacy of βEST and dFBr is greater at α4β2 nAChRs containing three copies of α4 subunit (**Figure 1**), suggesting α4 encodes the binding and transduction elements for βEST and dFBr potentiation. The α4β2 nAChR can assemble in two functional stoichiometries, one with three copies of α4 and two copies of β2 [$(\alpha4\beta2)_2\alpha4$] and the other with two copies of α4 and three copies of β2 [$(\alpha4\beta2)_2\beta2$] (20). The alternate receptors differ in pharmacological properties, including sensitivity to agonists and allosteric modulators (20, 21).

Previous studies have shown that βEST binds the post-M4 region of the α4 subunit (11). The site for dFBr binding has not been identified so far, although it has been suggested to lie within the ECD (22). Hence, to aid the identification of the potentiating dFBr binding site in the α4β2 nAChR, we performed docking stimulations with dFBr on a homology model of the α4β2 nAChR. Some docking positions were found in the pore, but the majority were found in the cavity between M3 and M4 of both the α4 subunit (**Figure 2A**) and the β2 subunit (not shown). The position of dFBr in the latter tended to be located more superficially to the cavity. The M3-M4 cavity is a common allosteric site in pLGICs and is the target of a wide variety of allosteric modulators such as general anaesthetics in anionic pLGICs (23-25), neurosteroids in $GABA_A$ receptors (26) and PNU-120596 and LY-2087101 in α7 nAChRs (27).

Note that during revision of this manuscript the X-ray structure of the $(\alpha4\beta2)_2\beta2$ nAChR in a presumed desensitised conformation was published (28). We overlaid our homology model and the X-ray structure of the $(\alpha4\beta2)_2\beta2$ receptors. This showed that the proposed dFBr binding region is fairly similar in both the

homology model and the X-ray structure of the $(\alpha4\beta2)_2\beta2$ receptor (**Figure 2B)** and demonstrates that our homology model is a valid tool to predict interactions between the α4β2 nAChR and ligands.

To elucidate which residues in the TMD of the α4 subunit might contribute to the putative dFBr binding site, we prioritized residues with their side chain pointing towards the cavity and individually substituted them with alanine. These studies highlighted α4 M3 Y309, F312, T313 and F316 and M4 L617 and F606 as residues that may interact with dFBr in the putative dFBr binding site to enhance, allosterically, the ACh responses of α4β2 nAChRs (**Figure 2A, B).**

The consequences of the alanine substitutions on dFBr potentiation were assessed on α4β2 nAChRs assembled from equal ratios of α4 and β2 cDNA. This was necessary to obviate potential problems in data analysis due to low levels of functional expression, which may occur when working with mutants of homogeneous populations of α4β2 nAChRs. The receptors obtained using equal ratios of cDNA consist of approximately 80-90% of $(\alpha4\beta2)_2\alpha4$ and 10-20% of $(\alpha4\beta2)_2\beta2$ receptors (20).

Functional assays revealed Y309, F312 and L617 as pivotal determinants of dFBr potentiation. Y309A and F312A abolished dFBr potentiation and increased dFBr $EC_{50,}$ compared to wild type **(Figures 2C; Table 1)**. L617A reduced the maximal potentiating effect of dFBr (dFBr efficacy) by 9.5-fold and dFBr EC_{50} by 7-fold ($p < 0.001$; n = 5), as compared to wild type **(Figures 2C; Table 1**). Increased polarity in these positions significantly affected dFBr potentiation. Thus, L617C decreased both dFBr efficacy (3.5-fold) and dFBr EC_{50} (6.7-fold) whereas F312C and Y309C obliterated the potentiating effects of dFBr (**Table 1**). To determine whether aromaticity at these positions is essential for dFBr potentiation, the effects of F312Y, Y309F and L617F on dFBr potentiation were examined. F312Y, Y309F and L617F reduced dFBr efficacy to similar levels. However, although L617F decreased dFBr EC_{50}, F312Y and Y309F increased it, compared to wild type (**Table 1**). None of the Y309, F312 and F167 mutants affected ACh EC_{50} (**Table 1**). Alanine or cysteine substitutions on T313, F316 or F606, which are predicted to lie below F312, also decreased dFBr efficacy and increased dFBr EC_{50} values, although their effects were less pronounced than those of Y309, F312 or L617 (**Table 1**). Substitutions on T313 did not affect sensitivity to activation by ACh (**Table 1**), but all substitutions engineered on F316 and F606 did (**Table 1**), suggesting that the effects of mutations on F316 and F606 on dFBr potentiation were a consequence of mutant-induced perturbation of receptor function.

To further confirm the role of the α4 subunit on dFBr potentiation of α4β2 nAChRs, and further establish that M3 encodes binding residues for dFBr, we introduced α4F312A sequentially into concatenated $(\alpha4\beta2)_2\alpha4$ and $(\alpha4\beta2)_2\beta2$ receptors. Concatenated receptors have fixed stoichiometry and subunit arrangement, and these constructs have been shown to replicate the functional properties of the receptors assembled from loose α4 and β2 subunits (21).

As expected, introducing α4F312A in the α4 subunit contributing the principal component of the agonist site on the α4/α4 subunit interface of the $(\alpha4\beta2)_2\alpha4$ receptor (29, 30) reduced the potentiating efficacy of dFBr to $(\alpha4\beta2)_2\beta2$-like levels (**Figure 2D**), and dFBr potency decreased from 1.8 ± 0.5 μM to 2.5 ± 0.1 μM ($p < 0.05$; n = 5), which is not different from the potency of dFBr on concatenated $(\alpha4\beta2)_2\beta2$ receptors. The additional agonist site on the $(\alpha4\beta2)_2\alpha4$ receptor receptors plays a dominant role in determining the signature properties of this receptor type, as compared to the $(\alpha4\beta2)_2\beta2$ receptor (29–31). When the additional agonist site is ablated, $(\alpha4\beta2)_2\alpha4$ receptor displays $(\alpha4\beta2)_2\beta2$-like pharmacology (30, 31), including sensitivity to agonists and allosteric modulators (11, 20, 21). Significantly, introducing α4F312A in one of the two agonist sites of the $(\alpha4\beta2)_2\beta2$ receptor reduced dFBr efficacy by approximately 50% (**Figure 2D**) and decreased dFBr potency to 12 ± 1 μM ($p < 0.001$; n =5). When the mutation was introduced in all copies of α4 in both receptor types, the receptors were no longer sensitive to potentiation by dFBr (**Figure 2D**). These findings indicate that pivotal determinants of dFBr potentiating potency and efficacy are encoded by the α4 subunit.

Effects of dFBr on MTSET reaction rates. Demonstrating that dFBr can access residues in the top half of the cavity between M3 and M4 of the α4 subunit would further support the conclusion that this region houses a dFBr potentiation site. We determined this by assessing the ability of dFBr to protect L617C from covalent modification by the thiol

compound MTSET (protection assays). L617C decreased the efficacy of dFBr but had no effects on ACh $EC_{50,}$ indicating that the observed changes in dFBr potentiation are not linked to changes in ACh EC_{50} (**Table 1**). Neither F312C nor Y309C were used for dFBr protection assays because these mutants abolished dFBr potentiation (**Table 1**). We first determined the accessibility of L617C to covalent modification by MTSET by exposing α4L617Cβ2 receptors to MTSET for 2 min following stabilisation of ACh EC_{10} responses. ACh-elicited responses and dFBr potentiation of ACh responses were measured before and after MTSET exposure (**Figure 3A**). MTSET had no effect on the ACh responses or dFBr potentiation (**Figure 3B**) of wild type receptors, indicating that any change measured in ACh responses or dFBr potentiation after MTSET exposure is due to MTSET-modification of L617C. Potentiation of ACh responses was abolished by MTSET, indicating that α4L617C is fully accessible to MTSET (**Figures 3A, B**). This effect is selective because MTSET treatment of α4F316C, which we propose perturbs dFBr potentiation of α4β2 receptors indirectly, reduced dFBr potentiation by only 30% (**Figure 3B**), indicative of limited accessibility to MTSET at this position. For the protection assays, we first stabilised the currents elicited by an EC_{10} concentration of ACh at α4L617Cβ2 receptors and then co-applied ACh EC_{10} with EC_{100} dFBr to test the maximal dFBr potentiation on α4L617Cβ2 receptors. Next, a sequence of applications (10 seconds) of 20 μM MTSET in the presence or absence of dFBr EC_{100} (10 μM) was tested for a total time of 40 seconds (**Figure 3C**). After each application ACh EC_{10} + dFBr EC_{100} responses were tested for changes in the amplitude of the responses (**Figure 3C**). The reaction rate of MTSET with α4L617C in the absence of dFBr was 12-fold faster (k_1 0.05 ± 0.01 s^{-1}) than in the presence of dFBr (k_1 0.004 ± 0.0 03 s^{-1}) ($p < 0.0001$; n = 4) (**Figure 3D**). Together, the findings show that dFBr protects L617C from reacting with MTSET, which would occur if dFBr binds the dFBr binding site in the top-half cavity between M3 and M4 in the α4 subunit.

Y309 and F312 are conserved in the β2 subunit (**Figure 4A**), and docking studies indicate that dFBr may bind in a narrow cavity between the top of M3 and M4 in β2 (not shown). We therefore tested whether Y300 and F303 in the β2 subunit, equivalents to α4Y309 and α4F312, respectively, altered the potentiating effects of dFBr on α4β2 receptors. Incorporation of β2F303A or β2Y300A decreased both dFBr efficacy and potency (**Table 1**). However, because β2Y300A and β2F303A markedly decreased ACh EC_{50} ($p < 0.0001$; n = 5), their effects on dFBr efficacy likely reflect perturbations to receptor function rather than direct effects on dFBr potentiation. The TMD of pLGICs play a pivotal role in gating, and structural integrity in some regions is critically important for this function (32-34).

Finally, it has been previously suggested that the potentiating binding site of dFBr is located in the β2+/α4- interface of the α4β2 nAChR and that key contributors to this site are β2 subunit residues W176, Y120, D217 and D218 (22). We performed alanine substitutions on these residues but found that none disturbed dFBr potentiation significantly (**Table 2**).

The Cys loop affects dFBr potentiation. Surprisingly, F312, Y309 and L617 are conserved in the α3 nAChR subunit (**Figure 4A**), yet α3β2 nAChRs were found to be only inhibited by dFBr (IC_{50} 118 ±5 μM; n = 6) (**Figure 4B**). Inhibition of α3β2 nAChRs by dFBr is not mediated by a site in the M3-M4 cavity because alanine substitution on α3F310, the α3 residue equivalent to the crucial F312 in the α4 subunit, has no effect on dFBr-mediated inhibition (IC_{50} 115 ±7 μM; n = 6) (**Figure 4B**). In addition, inhibition of α3β2 nAChRs is voltage-dependent (not shown) and the current responses to ACh EC_{10} in the presence of concentrations of dFBr greater than 10 μM rebound, strongly suggestive of ion channel blockade (**Figure 4B inset**). Together, these findings suggest that the α3 subunit may lack structural elements required for transducing the positive allosteric signals generated by binding of dFBr to the M3-M4 cavity. The agonist binding-gating coupling elements, the β1-β2 loop and the Cys loop, have been shown to contribute to the transduction of positive allosteric signals in α4β2 nAChRs (17). Importantly, α3 and α4 differ in five amino acid positions in these regions, two in loop β1-β2 and three in the Cys loop (**Figure 4A**). To determine whether these residue differences are defining factors for sensitivity to potentiation by dFBr, we mutated the α4 residues to their α3 counterparts. Neither mutating α4S162 in the Cys loop to lysine, its α3 equivalent, nor changing α4 loop β1-β2 into an α3 β1-β2 loop [α4(α3β1- β2 loop)] had any significant effect on dFBr potentiation (**Figure 4C, Table 3**). In

contrast, substituting F167 in the α4 subunit Cys loop with its α3 equivalent (a tyrosine) reduced the efficacy of dFBr by five-fold without changes in dFBr EC_{50} (**Figure 4C; Table 3**). In addition, alanine substitution of F167 had no effect on dFBr EC_{50} but almost abolished potentiation by decreasing dFBr efficacy by 9.6 fold (**Figure 4C; Table 3**).

F167 is next to the canonical FPF motif carried by the Cys loop in pLGICs, which interacts with neighbouring pre-M1 in the ECD and the M2-M3 linker in a well-established pathway linking agonist binding to channel gating (5, 6). We examined the relevance of FPF for dFBr potentiation by individual mutations on the α4 Cys loop motif (F168, P169, F170). Substitutions on proline (P169A, P169F, P169L) did not yield functional expression. Alanine substitution on F170 was well tolerated and decreased dFBr potentiation efficacy by 5.9 fold (**Figure 4C; Table 3**). Alanine substitution on F168 did not yield functional expression (not shown), and F168L, which did not affect the functional expression of α4β2 nAChRs, had no effect on dFBr potentiation (**Figure 4C; Table 3**).

The discovery that F167 and F170 are capable of influencing dFBr potentiation of α4β2 nAChRs suggest that the Cys loop may be part of the transduction mechanism for potentiation by dFBr. Interactions between the Cys loop and post-M4 are thought to be important for efficient gating of muscle nAChRs (8). To determine the relevance of α4 post-M4 (**Figure 4A**) for dFBr potentiation of α4β2 nAChRs, we first determined the effect of dFBr on receptors containing α4 subunits devoid of post-M4 (α4$^-$PM4). In accord with previous studies (35), we found that α4$^-$PM4β2 nAChRs were functional, albeit with reduced sensitivity to ACh, in comparison to wild type (**Table 3**). Significantly, removal of post-M4 reduced dFBr efficacy by 8.8-fold (**Figure 5A; Table 3**). To confirm the importance of post M4 for dFBr potentiation, we examined dFBr effects on α4LMAREDAβ2 nAChRs. α4LMAREDA comprises the ECD and TMD from the α4 subunit linked to α3 post-M4 (LMAREDA) (**Figure 4A**). If post-M4 in the α4 subunit is a key determinant of dFBr potentiation, α4LMAREDAβ2 nAChRs should not be potentiated by dFBr. As shown in **Figure 5A (Table 3)**, dFBr potentiation was ablated in α4LMAREDAβ2 nAChRs. To elucidate which α4 post-M4 amino acid residues (WLAGMI) are important for dFBr potentiation of α4β2 nAChRs, we examined the effects of dFBr on alanine mutants of the α4 post-M4 region. Individual alanine substitutions on the sequence WLAGM reduced potentiation but not significantly **(Figure 5A; Table 3**). In contrast, alanine substitution of the final residue of α4 subunit post-M4 (I626) abolished dFBr potentiation (**Figure 5A; Table 3**).

α4 M4 carries a double proline motif (PP) that precedes post-M4 (**Figure 4A**) that is conserved only in the α4 and α2 nAChR subunits, both of which are sensitive to dFBr potentiation (11, 36). The PP motif may introduce considerable restrictions on the orientation and mobility of post-M4, which could be pivotal for dFBr potentiation. To determine the relevance of the PP motif for dFBr potentiation, the prolines were mutated to alanine individually as well as simultaneously. As shown in **Figure 5A (Table 3)**, **AA**WLAGMI obliterated the potentiating effects of dFBr and **AP**WLAGMI or **PA**WLAGMI reduced potentiation by 9-fold. Furthermore, exchange of the PP motif for QP, the motif preceding post-M4 in the α3 subunit (**Figure 4A**), decreased dFBr potentiation by 8.2-fold (**Figure 5A; Table 3**).

To further confirm the relevance of post-M4 and the double PP motif for dFBr potentiation, we tested the effect of changing the α3 subunit QPLMAREDA region to the equivalent α4 region (PPWLAGMI). We had shown in this study that α3β2 nAChRs are inhibited by dFBr (**Figure 4B**), even though residues pivotal for potentiating dFBr binding in the α4 subunit are conserved in the α3 subunit (**Figure 4A**). If dFBr potentiation requires the binding site in the top-half of the cavity between M3 and M4 and the PPWLAGMI sequence, α3PPWLAGMIβ2 receptors should be sensitive to potentiation by dFBr. As shown in **Figure 5B-C**, α3PPWLAGMIβ2 nAChRs were potentiated by dFBr (I_{max} = 4 ± 0.2; EC_{50} 7 ±0.2 μM; n = 5), unlike wild type α3β2 nAChRs. Significantly, incorporation of F310A into α3PPWLAGMI abolished dFBr potentiation (I_{max} 0.99 ±0.06; n = 4; $p < 0.001$) (**Figure 5C**).

Interactions between post-M4 and Cys loop are necessary for dFBr potentiation. The atomic structure of post-M4 in pLGICs has not been resolved (e.g., 3, 4, 29). However, since it has been proposed that post-M4 in muscle nAChRs may interact with the Cys loop to modulate gating (8),we hypothesised that post-M4 extends towards the Cys loop and that

binding of dFBr to the M3-M4 cavity promotes interactions between F170 and I626 (**Figure 6A**), leading to potentiation of receptor function.

To test this possibility, we disrupted any possible functional interdependence by mutating the residues individually (F170I, I626F) and also in pairs (F170I-I626F) to potentially restore functional interdependence. Mutants F170I, I626F and F170I-I626F were well tolerated, all yielding functional expression. F170I and I626F reduced dFBr potentiation by 4.6-fold and 4.8-fold, respectively, as compared to wild type (**Figure 6B, E; Table 3**). When both mutations were present (F170I-I626F), dFBr potentiation was increased by 2.4-fold, in comparison to the single mutants (**Figure 6B; Table 3**). Moreover, dFBr efficacy was 1.2-fold higher than the sum of the dFBr efficacy at the individual mutants ($p < 0.01$, $n = 4$). If mutants F170I and I626F acted independently, the effect of the double mutation should be additive. We also examined whether the double proline could interact with F170 but mutants F170P, F170P-P620F and F170P-P626F did not yield functional expression.

We next examined the possible role of F167 in dFBr potentiation. F167 is close to L305 in the M2-M3 linker of the α4 subunit (**Figure 6A**), a residue that in the muscle nAChR is energetically coupled to the Cys loop and pre-M1 region to contribute to gating (*6*). α4F167L had no effect on dFBr potentiation, whereas L305F abolished it (**Figure 6C; Table 3**). When both mutations were present, dFBr potentiation was abolished (**Figure 6C; Table 3**), indicating that the effect of L305 on dFBr potentiation is not dependent on F167. The side chain of F167 is also predicted to orientate towards Y309 in M3 (**Figure 6A**). We established earlier that Y309 (**Figure 2B**) and F167 (**Figure 4C**) are critically important for dFBr potentiation. To determine whether F167 and Y309 contribute to dFBr potentiation interdependently, we mutated F167 to tyrosine and Y309 to phenylalanine, and examined the effects of these mutants on dFBr potentiation individually or in pair. F167Y and Y309F decreased dFBr efficacy by 4.8- and 3.8-fold, respectively, compared to wild type (**Figure 6D, E; Table 3**). When the mutations were introduced simultaneously (F167Y-Y309F), dFBr efficacy was restored to near wild type values (**Figure 6D, E; Table 3**).

F170 and I626 interactions are necessary for βEST potentiation. βEST is an established positive allosteric modulator of α4β2 nAChRs (11, 19, 35). Previous studies have shown that residues in α4 post-M4 are involved in both binding (AGMI, the last four residues of post-M4) and transduction (W621, the first post-M4 residue) of potentiating βEST (11, 35). As for dFBr potentiation, the potentiating efficacy of βEST is greater at (α4β2)2α4 receptors (**Figure 1A**). To assess whether the Cys loop - post-M4 interactions that affect dFBr potentiation are relevant for βEST potentiation, we assessed the effects of F170I and I626F on βEST potentiation, individually and in pairs. Individually, F170I and I626F abolished βEST potentiation (**Figure 7A; Table 4**). When both mutations were present (F170I-I626F), βEST efficacy was restored to near wild type values (**Figure 7A, Table 4**).

We also examined whether F167 and Y309 were relevant for βEST potentiation. Mutants F167Y, Y309F or F167Y-Y309F had no impact on βEST potentiation (**Figure 7B**). These results suggested that F167 and Y309 may affect selectively potentiation by compounds that bind the M3-M4 cavity. To examine this possibility, we assayed the effect of F167A, Y309A and F3212A on βEST potentiation. βEST potentiation was not affected by F167A, Y309A or F312A (**Table 4**). In contrast, alanine substitution on L617 abolished βEST potentiation (**Table 4**).

DISCUSSION

This study provides the first demonstration that interactions between the Cys loop and the post-M4 region of the α4 subunit affect potentiation of α4β2 nAChR function by PAMs that bind the TMD region of the α4 subunit. Our data reveal that in the α4 subunit F170 of the Cys loop and I626, the final residue of post-M4, are functionally coupled, and show that this coupling is essential to transduce binding of βEST and dFBr into potentiation of α4β2 nAChR function. This conclusion is based on the observation that individual residue swaps, F170I and I626F, ablated (βEST) or attenuated (dFBr) potentiation, whereas double mutant (F170I-I626F) restored potentiation to wild type values (βEST) or increased it above the levels expected from simple additivity (dFBr). In addition, individual alanine mutations on F170 and I626 also affected βEST and dFBr potentiation, in a manner consistent with annulment of the functional link between them. Significantly, transfer of the α4 subunit post-M4 region to the α3 subunit, which conserves the key dFBr binding residues in the TMD,

conferred sensitivity to dFBr potentiation to α3β2 nAChRs. A similar phenomenon has been reported for the potentiation of α4β2 nAChR by βEST (35).

Without structural data for α4 post-M4, it is not possible to infer any specific details about the structural framework that could account for F170/I626 functional interdependence and its role in dFBr and βEST potentiation. In the muscle nAChR structure, post-M4 extends beyond the lipid bilayer towards the Cys loop to seemingly interact with F137 (F170 in α4) (8). Moreover, the post-M4 residue that appears to interact with F137 is Q435, a residue that aligns with α4I626 (**Figure 4A**). The functional consequences of putative F137/Q435 interactions have not been examined so far, but it has been suggested that they may contribute to coupling agonist binding to channel gating, as well as transducing the allosteric effects of lipid binding to M4 (8). In regard of the α4β2 nAChR, localised motion transitions triggered by binding of PAMs to the TMD could promote F170-I626 gating interactions, leading to more efficacious agonist-triggered receptor activation. Given that M4 is covalently linked to post-M4, local structural changes induced by PAM binding to the M3-M4 cavity could be relayed to post-M4 through M4 motions. In accord with this possibility, we found dFBr and βEST may engage in binding interactions with M4 L617, and these binding interactions are likely to trigger M4 motions that could subsequently alter the orientation of post-M4. Significantly, NMR structures of the TMD of the α4β2 nAChR bound to allosteric inhibitors halothane or ketamine show that binding of these modulators to their binding sites in the TMD elicits changes in protein dynamics beyond the binding sites (37). Also, molecular dynamics simulations show the M4 as a structurally dynamic element undertaking substantial motion during muscle nAChR gating (38). Additionally, M4 is known to affect gating of the muscle nAChR (32) and, more recently, it has been proposed that enhanced interactions between M4 and M1-M3 promotes channel function in GLIC, a prokaryotic pLGIC (7).

Extensive mutagenesis studies of α4 post-M4 have led to the view that the final four residues of the α4 subunit bind βEST and that the C-terminus of the tail likely plays a role in transduction (35). In contrast, our data strongly suggests that the last residue of post-M4 (I626) functionally couples to F170 to transduce binding of βEST into receptor potentiation. Without structural data for post-M4 of the α4β2 receptor or adequate probes to photo-label the binding site for βEST, we cannot easily reconcile our findings with the view that βEST binds the tail of post-M4. However, our observation that substitutions of M4 L617 ablated βEST potentiation, suggests L617 may contribute to the βEST binding site, locating this site to the top part of M4. This would be in accord with the observation that neither F167 nor Y309 had any effects on βEST potentiation. Moreover, a binding site on the top of M4 would place the site nearby to F170 and I626, the crucial transduction components for this site.

An important finding of this study is that a cavity between the top half of the M3 and M4 of the α4 nAChR subunit hosts the potentiating binding site of dFBr. M3 (F312 and T313) and M4 (L617) residue side chains are predicted to project towards the M3-M4 cavity and reside sufficiently close to one another to all be able to bind dFBr. When their capacity to bind dFBr was annulled by alanine substitution, the sensitivity to dFBr potentiation was either abolished (as for F312A) or drastically reduced (as for L617A or T313). Moreover, protection assays with MTSET demonstrated that dFBr impeded accessibility of L617C by MTSET, suggesting that dFBr occupies the cavity towards which the side chain of residues L617, F312 and T313 orientates. This cavity is a common allosteric site in pLGICs and is the target of a wide variety of allosteric modulators such as general anaesthetics in anionic pLGICs (23-25), small neurosteroids in $GABA_A$ receptors (26) and PNU-120596 and LY-2087101 in α7 nAChRs (27). Alanine or cysteine substitutions on M3 F316 or M4 F606 also attenuated dFBr potentiation but their effects on ACh EC_{50} suggest these residues may affect dFBr potentiation indirectly by affecting channel gating. In support of this possibility, it has been reported that F316, a residue highly conserved in the α subunits of the nAChR family, affects gating in the muscle nAChR (33, 34) and M4 is well-established gating modulator domain (8, 34).

In addition to F170 and I626, which we suggest to be transducing elements linked to the binding sites of βEST and dFBr, F167 and Y309 were also identified as important components of the transduction of dFBr binding. Individually, mutants F167Y and Y309F drastically attenuated dFBr potentiation but the double mutant F167Y-

Y309F restored potentiation to wild type levels. Furthermore, individual alanine substitutions on these residues affected dFBr potentiation similarly, supporting the possibility of these two residues being involved functionally. Importantly, F167 is predicted to project downwards towards M3 to meet the side chain of Y309 that extends upwards, thus positioning the transduction complex nearby the dFBr site. Furthermore, F167 precedes the critical FPF gating motif. Thus, conceivably, F167-Y309 interactions could optimise the gating conformations of the Cys loop FPF motif, leading to enhanced receptor function.

As Y309 is not predicted to project towards F170, F167-Y309 interactions are unlikely to be part of the F170-I626 transducing pathway. Thus, analogously to the gating of the muscle nAChR, in which the β1-β2 and Cys loops appear to act jointly on the M2-M3 linker to gate the ion channel (6), dFBr binding is transduced by two independent pathways that act on the Cys loop to produce receptor potentiation. Compared to βEST, dFBr is approximately 7-fold more efficacious, thus suggesting that a functional consequence of F167-Y309 and F170-I626 dFBr-dependent interactions is greater potentiating efficacy.

Finally, given that the FPF motif of the Cys loop and M3 are highly conserved in the nAChR subunits that form heteromeric nAChRs (**Figure 4A**), the structural element that is pivotal in determining sensitivity to potentiation by dFBr and βEST is post-M4. In comparison to other α subunits that form heteromeric receptors insensitive to dFBr potentiation (e.g., muscle nAChR, α3β2 nAChR), post-M4 in α4 is more hydrophobic, suggesting that it could extend more easily towards the hydrophobic ECD/TMD coupling region than less hydrophobic M4 tails. Furthermore, the presence of the signature double proline motif preceding α4 post-M4 likely places considerable constraint on the orientation of post-M4, perhaps anchoring post-M4 to the membrane underneath the Cys loop FPF motif, thereby aiding interactions of this domain with the F170 in the Cys loop. In accord with this view, double or individual alanine substitutions on PP severely attenuated (AP or PA) or ablated (AA) dFBr potentiation.

The transduction mechanism presented here for PAM binding sites in the TMD of the α4β2 nAChR provides strong experimental evidence that interactions between the TMD and the Cys loop are critical for allosteric modulation of pLGICs by PAMs. Thus, in addition to its role in coupling agonist-binding to channel gating, the Cys loop also couples TMD to the channel gate. The Cys loop is thus a hub that conveys gating signals to the channel gates from both the ECD and the TMD.

EXPERIMENTAL PROCEDURES

Materials. DFBr was purchased from Tocris Chemicals (UK) and βEST from Sigma-Aldrich, UK. The cationic methanethiolsulfonate reagent [2-(Trimethylammonium) ethyl] methanethiosulfonate (MTSET) was purchased from Toronto Chemicals (Canada). 100 mM stocks were prepared and stored at -80 C°. Just before use, MTSET stocks were diluted to the appropriate concentration in Ringer's solution and were applied immediately to the oocytes. *Xenopus laevis* (*X. laevis*) were purchased from Portsmouth University (Portsmouth, UK) or *Xenopus*-One (Chicago, USA). Ovaries were dissected from the toads using procedures in accordance with the UK Home Office regulations.

Molecular Biology. Human cDNA of the α4 and β2 subunits were cloned into the expression vector pCI (Promega), whilst the α3 nAChR subunit cDNA (kindly provided by Prof L Sivilotti from UCL, London, UK) was cloned into pcDNA3.1 (Invitrogen). Site directed mutagenesis was performed using the QuikChange mutagenesis kit (Stratagene, Europe). The full-length sequence of mutant subunit cDNAs was verified by DNA sequencing (BioSource Sequencing, Oxford and Eurofins-MWG, Germany). We present the numbering of the residues in terms of the full length, including the signal sequence. To obtain the position in the mature form, subtract 28 from the number for α4, 25 for β2 and 31 for α3.

Expression of nAChR in Xenopus Oocytes. Stage V and VI *Xenopus* oocytes were prepared as previously described (10). Wild type or mutant human α4 or α3 subunit cDNAs were co-injected with β2 subunit cDNA into the nuclei of oocytes in a volume of 18.4 nl/oocyte at equal ratios, using a Nanoject Automatic Oocyte Injector (Drummond, Broomall, PA, USA). The total amount of cDNA injected per oocyte was kept constant at 2 ng. After injection, oocytes were incubated at 18 °C for 2-5 days in a modified Barth's solution containing 88 mM NaCl, 1 mM KCl, 2.4 mM $NaHCO_3$, 0.3 mM $Ca(NO_3)_2$, 0.41 mM $CaCl_2$, 0.82 mM $MgSO_4$, 15 mM HEPES and 5 mg/l neomycin (pH 7.6).

Equal ratios of α4 and β2 subunits yields a mixture of two functional stoichiometries, $(\alpha4\beta2)_2\alpha4$ and $(\alpha4\beta2)_2\beta2$. These two receptor types have distinct pharmacological properties, including sensitivity to activation by ACh (20). To test the effects of dFBr in the alternate α4β2 receptors, we expressed fully concatenated receptors. We have shown previously that concatenated α4β2 receptors replicate the properties of their non-linked counterparts (21). Concatenated receptors were constructed as α4β2 receptors as previously described (21). To introduce mutations into the subunits of the concatemers, the mutations were first introduced in free subunits cloned into a modified pCI plasmid (Promega, UK) and, following sequence verification by double stranded DNA sequencing (SourceBioscience, Oxford, U. K), the subunits were ligated to the desired position in the concatemer using unique enzyme restriction sites (21). To verify that the mutated subunits were incorporated into the concatenated receptors, following ligation and DNA amplification, the mutated subunit were excised enzymatically from the concatemer for sequence verification by double stranded DNA sequencing (SourceBioscience, Oxford, U. K).

Electrophysiology and Concentration Response Curves. Recordings were performed 2 - 5 days post-injection, as previously described (10). Briefly, oocytes were placed in a 0.1 ml recording chamber and perfused with modified Ringer's solution (in mM: NaCl 150, KCl 2.8, HEPES 10, $CaCl_2$ 1.8; pH 7.2, adjusted with NaOH) at a rate of 15 ml/min. Note that it has been reported that $(\alpha4\beta2)_2\beta2$ nAChRs are potentiated by HEPES, possibly by binding a site in the signature β2/β2 interface of this receptor type (39). We have tested the effects of HEPES on the function of $(\alpha4\beta2)_2\beta2$ nAChRs and found no effects. Moreover, we compared the sensitivity of $(\alpha4\beta2)_2\beta2$ and $(\alpha4\beta2)_2\alpha4$ nAChRs to ACh, Zn^{2+}, dFBr and βEST using Ringer solutions buffered by HEPES or phosphate buffer and found no differences (not shown). In accord with these findings, the recently published X-ray structure of the $(\alpha4\beta2)_2\beta2$ nAChRs suggests ligands may not access the β2/β2 interface easily (28). Current responses were obtained by two-electrode voltage-clamp recording at a holding potential of -60 mV using an Oocyte Clamp OC-725C amplifier (Warner Instruments, USA) and Labscribe software (Iworx, NH, USA). Electrodes contained 3 M KCl and had a resistance of < 1 MΩ. ACh, dFBr and βEST were prepared daily in Ringer's solution from frozen stocks (10 mM). All experiments were carried out at room temperature. For wild type and mutant α4β2 or α3β2 nAChR, a 6 to 7 point concentration-response curve was generated for ACh alone or with allosteric modulators (dFBr or βEST). Peak currents for ACh were normalised to the currents elicited by 1 mM (ACh EC_{100}). Allosteric modulators were co-applied with ACh EC_{10} for the receptor under study and the peak current responses were normalised to the responses elicited by ACh EC_{10} alone. Oocytes were superfused with Ringer's solution for 5 min between all drug applications. To eliminate data interpretation or analysis arising from run-up or run-down of current responses over the course of experiments, all oocytes were initially stabilised with ACh EC_{100}. Oocytes were discarded if the response to ACh EC_{100} varied by more than ± 10%.

Substituted Cysteine Accessibility Method. Accessibility of introduced cysteines to MTSET was determined by exposing the cysteines to a maximal concentration of MTSET (1 mM) (40). Briefly, oocytes were stabilized before addition of MTSET by application of ACh and ACh + dFBr at 5-min intervals until the ACh-activated currents (I_{ACh}) and dFBr potentiation of I_{ACh} varied by less than 6%. ACh concentrations used were EC_{10} and dFBr concentration used was EC_{100} for each mutant. After the ACh and dFBr responses were stabilized, freshly diluted 1 mM MTSET was applied for 2 min, the cell was washed for 5 min, and then ACh and ACh + dFBr responses were measured. The effect of MTSET on dFBr potentiation of ACh responses was calculated as % Change = $[(I_{after}/I_{initial}) - 1) \times 100]$, where $I_{initial}$ is the response to ACh EC_{10} + dFBr EC_{100} prior to MTSET application and I_{after} is the response to ACh EC_{10} + dFBr EC_{100} after MTSET application. After MTSET reactions, oocytes were exposed to the redox reagent 1, 4 dithiothreitol (1 mM, 2 min) to confirm that any changes observed were the result of covalent modification of the substituted residues by MTSET.

Rate of MTSET Modification. The rate of MTSET covalent modification of introduced cysteines was determined by measuring the effect of sequential applications of sub saturating MTSET (20 μM) on potentiation of EC_{10} ACh responses by EC_{100} dFBr. Following stabilisation

of dFBr potentiation of ACh responses, MTSET was applied for 5 s and the cell was then washed for 70 s and the procedure was repeated until changes in dFBr potentiation reached a plateau. Before the reaction rate was measured, ACh and ACh + dFBr were applied every 3.7 min until the response varied by less than 5%. The effects of dFBr on the rate of MTSET modification was tested by co-applying MTSET with EC_{100} dFBr. The change in current was plotted versus cumulative time of MTSET exposure. Peak values at each time point were normalized to the initial peak at time 0 s, and the data points were fit with a single-exponential decay function: $y = \text{span} \times e^{-kt} + \text{plateau}$ (Graph Pad Software), where k is the first pseudo-first order rate constant of the reaction. Plateau is the peak ACh current at the end of the reaction and Span is 1 – plateau.

Homology Modelling and Docking. Homology models of the α4β2 nAChRs were constructed using MODELLER 9.12 (41) and were based on the 5-HT_3 receptor X-ray structure (PDB ID: 4PIR) at 3.5 Å resolution (42). The template X-ray structure comprises the ECD, the TMD and part of the intracellular domain. Four residues are missing in the extracellular M2-M3 loop, and more than 60 residues are missing in the intracellular linker between M3 and M4. Sequences of the human α4 and β2 nAChR subunits were obtained from the ExPASy proteomics server with accession numbers P43681 (α4) and P17787 (β2) and aligned to the 5-HT_3R subunits using the alignment function of MODELLER (align2d) and, for comparison, also using two different alignment tools from the European Bioinformatics Institute (EBI), EMBOSS Stretcher and EMBOSS Needle, respectively. The sequence identity is 25% and the sequence similarity is approximately 45%. The three alignments were compared and the final alignment constructed with manual changes in regions where the alignment algorithms were not optimal. Disulphide bonds were included and 50 models for each of $(\alpha4)_3(\beta2)_2$ (α4-β2-α4-β2-α4) and $(\alpha4)_2(\beta2)_3$ (α4-β2-α4-β2-β2) were constructed. The models mainly varied in regions where the template was missing, and the best models were chosen based on analysing the MODELLER scores (molpdf, DOPE and GA341). The 3-4 best models in terms of all of these scores were further assessed with QMEAN (43) and the best QMEAN scoring model from this process was chosen as the appropriate model for docking. The template is missing for the C-terminal four residues of post-M4, and there residues are therefore not included in any of the generated models.

A 3D model of dFBr was constructed in Maestro version 9.7 (Schrödinger, LLC, New York, NY, 2012 (academic version) in both positively charged and neutral state. Protein and ligand models were prepared for docking using Autodock Tools (44) and docking calculations were performed with Autodock Vina (45). A large box of 74x74x40 $Å^3$ centered in the extracellular half of the ion channel and covering a large part of the TMD of all five chains was used as the search space for docking calculations. 20 binding models were generated for each ligand docked into each protein model, i.e. 80 poses were generated in total. The binding models were analysed visually as the docking scores were all very similar (best score among 80 posed was -7.5 and the worst -6.2).

Data Analysis. Concentration-response data analysis was performed using nonlinear regression analysis using Prism 5 software (Graph Pad, CA, USA). For simplicity ACh concentration-response curves were fit to a monophasic three-parameter Hill equation using GraphPad 5, although α4β2 nAChRs assembled from equal ratios of α4 and β2 cDNA yield biphasic ACh concentration-response curves (11). Concentration-response curves for the potentiating effects dFBr or βEST were also fit to the monophasic form of the Hill equation. Hill equation parameters, MTSET accessibility and MTSET rate constants were analysed by one-way analysis of variance (ANOVA), followed by a Dunnett post Hoc test. P values of < 0.05 were considered as significantly different

.

Acknowledgements: We thank Professor JH Steinbach (Washington University, Saint Louis, Missouri, USA) for valuable comments and criticisms. The work was supported by Oxford Brookes University funding to CA and SM. MM was funded by the Leverhulme Trust (RPG-059) and the Alfred Benzon Foundation. PIV and MF were funded by CONYCIT (1150615).

Conflicts of interest: The authors declare that they have no conflicts of interest with the contents of this article.

Author contributions: IB designed and coordinated the study. CA, IB, MM and PB wrote the paper. CA, TM and IB performed and analysed electrophysiological experiments. CA and SM designed and performed SCAM experiments. MM and PB constructed the homology model and performed docking experiments. PI and MF performed docking experiments. All authors approved the final version of the manuscript.

References

1. Cecchini, M., and Changueux, J-P. (2015) The nicotinic acetylcholine receptor and its prokaryotic homologues: structure, conformational transitions and allosteric modulation. *Neuropharm*. **96**, 137-149.
2. Unwin, N. (2005) Refined structure of the nicotinic acetylcholine receptor at 4Å resolution. *J. Mol. Biol*. **346**, 967-89.
3. Unwin, N., and Fujiyoshi, Y. (2012) Gating movement of acetylcholine receptor caught by plunge-freezing. *J. Mol. Biol*. **422**, 617-634.
4. Lee, W.Y., and Sine, S.M. (2005) Principal pathway coupling agonist binding to channel gating in nicotinic receptors. *Nature* **438**, 243-247.
5. Jha, A., Cadugan, D.J., Purohit, P., and Auerbach, A. (2007) Acetylcholine receptor gating at extracellular transmembrane domain interface: the Cys- loop and M2-M3 linker. *J Gen. Physiol*. **130**, 547-58.
6. Lee, W.Y., Free, C.R., and Sine, S.M. (2009) Binding to gating transduction in nicotinic receptors: Cys-loop energetically couples to pre-M1 and M2-M3 regions. *J. Neurosci*. **29**, 3189-3199.
7. Carswell. C. L., Hénault, C. M., Murlidaran, S., Therien, J. P., Juranka, P.F., Surujbali, J. A., Brannigan, G., Baenzinger, J. E. (2016) Role of the fourth transmembrane α helix in the allosteric modulation of pentameric ligand-gated ion channels. *Structure* **23**,1-10.
8. daCosta, C. J. B., and Baenziger, J. E. (2009) A lipid-dependent uncoupled conformation of the acetylcholine receptor. *J. Biol. Chem*. **284**, 17819-17825.
9. Hsiao, B., Dweck, D., and Luetje, C.W. (2001) Subunit-dependent modulation of neuronal nicotinic receptors by zinc. *J. Neurosci.* **21**, 1848-18856.
10. Moroni, M., Vijayan, R., Carbone, A., Zwart, R., Biggin, P. C., and Bermudez, I. (2008) Non-agonist-binding subunit interfaces confer distinct functional signatures to the alternate stoichiometries of the α4β2 nicotinic receptor: an α4-α4 interface is required for Zn^{2+} potentiation. *J. Neurosci*. **28**, 6884-6894.
11. Paradiso, K., Zhang, J., and Steinbach, J. H. (2001) The C terminus of the human nicotinic alpha4beta2 receptor forms a binding site required for potentiation by an estrogenic steroid. *J. Neurosci*. **21**, 6561-6580.
12. Sala, F., Mulet, J., Reddy, K. P., Bernal, J. A., Wikman, P., Valor, L. M., Peters, L., König, G. M., Criado, M., and Sala, S. (2005) Potentiation of human α4β2 neuronal nicotinic receptors by a *Flustra foliacea* metabolite. *Neurosci. Lett.* **373**, 144-149.
13. Weltzin, M. M., and Schulte, M. K. (2010) Pharmacological characterization of the allosteric modulator desformylflustrabromine and its interaction with α4β2 neuronal nicotinic acetylcholine receptors. *J. Pharmacol. Exp. Ther*. **334**, 917-926.
14. Hamouda, A. K., Deba, F., Wang, Z.J., and Cohen, J. B. (2016) Photolabeling a nicotinic acetylcholine receptor (nAChR) with an $(\alpha4)_3(\beta2)_2$ nAChR-selective positive allosteric modulator. *Mol. Pharmacol*. **89**, 575-584.
15. Broad, L. M., Zwart, R., Pearson, K. K., Lee, M., Wallace, L., McPhie G. I., Emkey, R., Hollinshead, S. P., Dell, C. P., Baker, S. R., and Sher, E. (2006) Identification and pharmacological profile of a new class of selective nicotinic acetylcholine receptor potentiators. *J. Pharmacol. Exp. Ther*. **318**, 1108-1117.
16. Timmermann, D. B., Sandager-Nielsen, K., Dyhring, T., Smith, M., Jacobsen, A-M., Nielsen, E.Ø., Grunnet, M., Christensen, J. K., Peters, D., Kohlhaas, K., Olsen, G. M., and Ahring, P. K. (2012) Augmentation of cognitive function by NS9283, a stoichiometry-dependent

positive allosteric modulator of α2- and α4-containing nicotinic acetylcholine receptors. *Brit. J. Pharmacol*. **167**, 164-182.

17. Olsen, J. A., Kastrup, J. S., Peters, D., Gajhede, M., Balle, T., and Ahring, P. K. (2013) Two distinct allosteric binding sites at α4β2 nicotinic acetylcholine receptors revealed by NS206 and NS9283 give unique insights to binding activity-associated linkage at Cys-loop receptors. *J. Biol. Chem*. **288**, 35997-36006.
18. Changeux, J-P. (2013) 50 years of allosteric interactions: the twists and turns of the models. *Nat. Rev. Mol. Cell. Biol*. **14**, 819-829.
19. Jin, X., and Steinbach, J. H. (2015) Potentiation of neuronal nicotinic receptors by 17β-estradiol: Role of the carboxy-terminal and the amino-terminal extracellular domain. *PLoS One* **10,** e0144631.
20. Moroni, M., Zwart, R., Sher, E., Cassels, B. K., and Bermudez, I. (2006) α4β2 nicotinic receptors with high and low acetylcholine sensitivity: pharmacology, stoichiometry, and sensitivity to long-term exposure to nicotine. *Mol. Pharmacol*. **70**, 755–768.
21. Carbone, A. L., Moroni, M., Groot-Kormelink, P. J., and Bermudez, I. (2009) Pentameric concatenated (alpha4)(2)(beta2)(3) and (alpha4)(3)(beta2)(2) nicotinic acetylcholine receptors: subunit arrangement determines functional expression. *Br. J. Pharmacol*. **156**, 970-981.
22. Weltzin, M. M., and Shultze, M. K. (2015) Desformylflustrabromine modulates α4β2 neuronal nicotinic acetylcholine receptor high- and low-sensitivity isoforms at allosteric clefts containing the β2 Subunit. *J. Pharmacol. Exp. Ther*. **354**, 184-194.
23. Nury, H., van Renterghem, C., Weng, Y., Tran, A., Baaden, M., Dufresne, V., Changeux, J-P., Sonner, J. M., Delarue, M., and Corringer, P-J. (2011) X-ray structures of general anaesthetics bound to a pentameric ligand-gated ion channel. *Nature* **469**, 428-431.
24. Jayakar, S. S., Dailey, W. P., Eckenhoff, R.G., and Cohen, J. B. (2013) Identification of propofol binding sites in a nicotinic acetylcholine receptor with a photoreactive propofol analog. *J. Biol. Chem*. **288**, 6178-6189.
25. Sauguet, L., Howard, R. J., Malherbe, L., Lee, U. S., Corringer, P-J., Harris, R. A., and Delarue, M. (2013) Structural basis for potentiation by alcohols and anaesthetics in a ligand-gated ion channel. *Nature Commun*. **4**, 1697.
26. Hosie, A. M., Wilkins, M. E., da Silva, H. M. A., and Smart, T. G. (2006) Endogenous neurosteroids regulate $GABA_A$ receptors through two discrete transmembrane sites. *Nature* **444**, 486-490.
27. Young, G. T., Zwart, R. T., Walker, A. S., Sher, E., and Millar, N. S. (2008) Potentiation of alpha 7 nicotinic acetylcholine receptors via an allosteric transmembrane site. *Proc. Natl. Acad. Sci. USA* **105**, 14686-14691.
28. Morales-Perez, C. L., Noviello, C. M., and Hibbs, R. E. (2016) X-ray structure of the human α4β2 nicotinic receptor. *Nature* 10.1038/nature19785.
29. Harpsøe, K., Ahring, P. K., Christensen, J. K., Jensen, M. L., Peters, D., and Balle, T. (2011) Unraveling the high- and low-sensitivity agonist responses of nicotinic acetylcholine receptors. *J Neurosci* **31,** 10759–10766.
30. Mazzaferro, S., Benallegue, N., Carbone, A., Gasparri, F., Vijayan, R., Biggin, P. C., Moroni, M., and Bermudez, I. (2011) An additional ACh binding site at the α4(+)/α4(-) interface of the $(α4β2)_2α4$nicotinic receptor influences agonist sensitivity. *J. Biol. Chem*. **286**, 31043-31054.
31. Mazzaferro, S., Gasparri, F., New, K., Alcaino, C., Faundez, M., Iturriaga-Vasquez, P., Vijayan, R., Biggin, P. C., and Bermudez, I. (2014) Non-equivalent ligand selectivity of agonist sites in (α4β2)2α4 nicotinic acetylcholine receptors: a key determinant of agonist efficacy. *J. Biol. Chem*. **289**, 21795–21806.
32. Bouzat, C., Barrantes, F., and Sine, S. (2000) Nicotinic receptor fourth transmembrane domain: hydrogen bonding by conserved threonine contributes to channel gating kinetics. *J. Gen. Physiol*. **115**,663-672.
33. De Rosa, M. J., Rayes, D., Spitzmaul, G., and Bouzat, C. (2002) Nicotinic receptor M3 transmembrane domain: position 8' contributes to channel gating. *Mol. Pharmacol*. **62**, 406-414.
34. Cadugan, D. J., and Auerbach, A. (2007) Conformational dynamics of the alpha M3

transmembrane helix during acetylcholine receptor channel gating. *Biophys*. **93**, 859-865.
35. Jin, X., and Steinbach, J. H. (2011) A portable site: a binding element for 17β-estradiol can be placed on any subunit of a nicotinic α4β2 receptor. *J. Neurosci*. **31**, 5045-5054.
36. Pandya, A., and Yakel, J. L. (2011) Allosteric modulator desformylflustrabromine relieves the inhibition of α2β2 and α4β2 nicotinic acetylcholine receptors by β-amyloid (1-42) peptide. *J. Mol. Neurosci*. **45**, 42-47.
37. Bondarenko, V., Mowrey, D., Liu, L.T., Xu, Y., and Tang, P. (2013) NMR resolved multiple anesthetic binding sites in the TM domains of the α4β2 nAChR. *Biochim. Biophys. Acta* **182**, 398-404.
38. Mitra, A., Bailey, T.D., and Auerbach, A. L. (2004). Structural dynamics of the M4 transmembrane segment during acetylcholine receptor gating. *Structure* **12**, 1909–1918.
39. Weltzin, M. M., Huang, Y., and Schulte, M. K. (2014) Allosteric modulation of alpha4beta2 nicotinic acetylcholine receptors by HEPES. *Eur. J. Pharmacol*. **732**, 159-168.
40. Zhang, H., and Karlin, A. (1997) Identification of acetylcholine receptor channel-lining residues in the M1 segment of the β-subunit. *Biochem*. **36**, 15856-1586.
41. Šali, A. and Blundell, T. L. (1993) Comparative protein modelling by satisfaction of spatial restraints. *J. Mol. Biol*. **234**, 779-815.
42. Hassaine, G., Deluz, C., Grasso, L., Wyss, R., Tol, M. B., Hovius, R., Graff, A., Stahlberg, S., Tomizaki, T., Desmyter, A., Moreau, C., Li, X. D., Poitevin, F., Vogel, H., and Nury, H. (2014) X-ray structure of the mouse 5-HT3 receptor. *Nature* **512**, 276-281.
43. Benkert, P., Biasini, M., and Schwede, T. (2010) Towards the estimation of the absolute quality of individual protein structure models. *Bioinformatics* **27**,343-350.
44. Morris, G. M., Huey, R., Lindstrom, W., Sanner, M.F., Belew, R. K., Goodsell, D.S., and Olson, A. J. (2009) Autodock4 and AutoDockTools4: automated docking with selective receptor flexibility. *J. Comput. Chem*. **30**, 2785-2791.
45. Trott, O., and Olson, A. J. (2010) AutoDock Vina: improving the speed and accuracy of docking with a new scoring function, efficient optimization, and multithreading. *J Comput. Chem*. **31**, 455-461.

Footnotes

Non-standard abbreviations. 17β-Estradiol, βEST; desformylflustrabromine, dFBr; extracellular domain, ECD; positive allosteric modulator, PAM; pentameric ligand gated ion channels, pLGICs; nicotinic acetylcholine receptor, nAChR; methanesulphonate reagent, MTS; [2-(Trimethylammonium) ethyl] methanethiosulfonate, MTSET; substituted cysteine accessibility method, SCAM; transmembrane domain, TMD

Table 1. Concentration effects of ACh and dFBr on wild type and mutant α4β2 nAChRs. The concentration effects of dFBr were determined on ACh responses elicited by EC_{10} ACh concentrations. The data points were used to generate concentration response curves from which EC_{50}, Hill coefficient (nH) (not shown) were estimated, as described in Experimental Procedures. Maximal potentiation by dFBr of ACh EC_{10} current responses ($I_{max\ pot}$) was calculated as ($I_{ACh\ EC10}$ + dFBr) /$I_{ACh\ EC10}$. Values represent the mean ± SEM of n number of experiments. Asteriks indicate that the change in EC_{50} or $I_{max\ pot.}$ is statistically significant (*, $p < 0.05$; **, $p < 0.001$, ***, $p < 0.0001$), as measured by one-way ANOVA with Dunnett's correction.

A4 TMD	Receptor	ACh		DFBr		
		EC_{50} (μM)	n	EC_{50} (μM)	$I_{max\ pot}$	n
	α4β2	100± 7	20	1.33±0.03	10.6±2.0	15
3	α4Y309Aβ2	116±19	8	0.0±0***	1.01±0.03***	9
	α4Y309Cβ2	109±16	6	0.0±0***	1.02±0.06***	7
	α4Y309Fβ2	115±5	4	0.4±0.1*	2.75±0.3*	6
	α4F312Aβ2	102±6	15	0.0±0***	1±0.001**	12
	α4F312Yβ2	113±16	8	0.26±0.09*	2.4±0.8*	6
	α4F312Cβ2	93±10	9	0.0±0***	1.04±0.06**	8
	α4T313Aβ2	123±7	9	1.8±0.3*	2.2±0.4**	9
	α4T313Cβ2	131±15	4	1.98±0.3*	2.91±0.4**	4
	α4F316Aβ2	161±30*	8	2.22±0. 04**	3.9±0.3**	8
	α4F316Cβ2	124±1*	4	2.5±0.1*	4.2±0.4**3	4
4	α4L617Aβ2	118±18	4	11±3*	1.11±0.4**	5
	α4L617Cβ2	120±7	4	10.84±2*	3±0.21**	4
	α4L617Fβ2	80±12	6	16.5±5*	1.21±0.2**	7
	α4F606Aβ2	51±12***	4	2.32±0.08***	3.8±1.2**	5
	α4F606Cβ2	131±8*	5	1.81±0.3*	4.01±1.4**	5
β2 TMD 3	α4β2Y300A	43±3***	3	6±3*	4.3±2*	3
	α4β2F303A	30±1.2***	5	8±2*	3.4±0.4*	4

Table 2. Concentration effects of ACh and dFBr on α4β2 nAChRs containing alanine substitutions on residues of the β2 ECD. The concentration effects of dFBr were determined on ACh responses elicited by EC_{10} ACh concentrations. The data points were used to generate concentration response curves from which EC_{50}, Hill coefficient (nH) (not shown) and maximal potentiation by dFBr of ACh EC_{10} current responses ($I_{max\ pot.}$) were estimated, as described in Experimental Procedures. Maximal potentiation by dFBr of ACh EC_{10} current responses ($I_{max\ pot}$) was calculated as ($I_{ACh\ EC10}$ + dFBr) /$I_{ACh\ EC10}$.Values represent the mean ± SEM of n number of experiments. All residues mutated to alanine and tested for functional effects on dFBr potentiation are predicted to lie within loops A, B or C of the ECD of the β2 subunit. None of the parameters estimated from the concentration response curves for DFBr were statistically different from their wild type counterparts (one-way ANOVA with Dunnett's correction). However, ACh EC_{50} values were shifted to the right with mutations Y120A, D217A and D218A producing significant shifts (*, $p < 0.05$). Of note, residues Y120 and W176 have been proposed to contribute to a potentiating dFBr-binding site (22).

	Receptor	**ACh**		**dFBr**		
		EC_{50} (μM)	**n**	**EC_{50} (μM)**	**$I_{max\ pot}$**	**n**
ECD Loop	α4β2	100± 7	20	1.33±0.03	10.6±2.0	15
A	α4β2Y120A	156± 36*	3	0.91±0.3	7.7±3	3
B	α4β2W176A	188± 31	5	1.61±0.09	7.8±2	3
	α4β2T177A	113± 12	4	1.12±0.1	6.7±2	3
C	α4β2Y221A	118± 15	3	1.11±0.1	12.8±2	3
	α4β2D217A	146± 22*	3	2.0±0.7	8.54±2	3
	α4β2D218A	138± 22*	4	2.1±0.2	10.12±2	3
	α4β2S219A	116± 10	4	1.7±0.3	9.8±2	3

Table 3. The Cys loop and post-M4 are necessary for dFBr potentiation of α4β2 nAChRs. EC_{50}, values were estimated from ACh or dFBr concentration response curves, as described in Experimental Procedures. Maximal potentiation by dFBr of ACh EC_{10} current responses ($I_{max\ pot}$) was calculated as $(I_{ACh\ EC10} + dFBr)/I_{ACh\ EC10}$. Values are expressed as the mean ± SEM on number of experiments. Statistical differences were determined using one-way ANOVA with Dunnett's correction. Asteriks denote levels of statistical differences: *, $p < 0.05$; **, $p < 0.001$.

Receptor	ACh		dFBr		
	EC_{50} (μM)	n	EC_{50} (μM)	$I_{max\ pot}$	n
α4β2	100± 7	20	1.33±0.03	10.6±2.0	15
α4(α3β1-β2 loop)β2	115± 16	5	1.81±0.3	8.8±3	6
α4F167Aβ2	142± 15*	4	1.6±0.5	1.1 ±0.05**	8
α4F170Aβ2	86±14	6	3.4±0.5**	1.8±0.09**	8
α4F168Lβ2	89±21	3	0.59±0.07	14.7±2	4
α4 PM4β2	118± 12	8	ND	1±0.07**	4
α4LMAREDAβ2	121± 15	6	ND	1.05±0.09**	5
α4W621Aβ2	107±20	3	1.7±0.4	7.6±2	5
α4L622Aβ2	101±26	3	2.0±0.8	9.1±3	4
α4M625Aβ2	110±15	3	1.9±0.4	5.7±1	6
α4I626Aβ2	115±10	3	ND	1.01±0.2**	6
α4AAWLAGMIβ2	126±12	3	ND	1.03±0.01**	5
α4APWLAGMIβ2	133±17	5	7.7±1***	1.3±0.02**	4
α4PAWLAGMIβ2	121±12	5	ND	1.1±0.09**	6
α4QPWLAGMIβ2	125±10	4	ND	1.3±0.09**	4
α4F170Iβ2	122±10	6	6.6±2**	2.3±0.23*	9
α4I626Fβ2	108±17	3	1.76±0.09	2.1±0.16*	7
α4F170I-I626Fβ2	110±25	6	3.5±0.9*	5.4±0.38**	9
α4F167Lβ2	91±15	4	2.94±0.8	10.82±0.42	5
α4L305Fβ2	104±23	4	ND	1±0.1**	6
α4F167L-L305Fβ2	125±22	5	ND	1±0.09**	7
α4Y309Fβ2	115±5	3	0.4±0.1	2.75±0.3*	7
α4F167Yβ2	95±9	3	1.4±0.2	2.2±0.17*	9
α4F167Y-Y309Fβ2	115±20	5	1.82±0,1	11.32±0.4	6

Table 4. Functional effects of βEST on ACh responses of α4β2 nAChRs. EC_{50}, Hill slope (not shown) and maximal potentiation by βEST ($\mathbf{I_{\beta EST\ max\ pot}}$) were estimated from concentration response curves, as described in Experimental Procedures. $\mathbf{I_{\beta EST\ max\ pot}}$ of ACh EC_{10} current was calculated as $(I_{ACh\ EC10} + \beta EST) / I_{ACh\ EC10}$. Values represent the mean ± SEM of n number of experiments. Statistical differences were determined using one-way ANOVA with Dunnett's correction. Asteriks show levels of statistical differences: * $p < 0.05$; **, $p < 0.001$.

nACh subunit	ACh		β-Estradiol		
	EC_{50} (μM)	n	EC_{50} (μM)	$I_{\beta EST\ max\ post}$	n
α4β2	100± 7	20	10.54±4	1.58±0.09	5
α4Y309Aβ2	116±19	8	12±5	1.48±0.3	3
α4F312Aβ2	102±6	15	13±5	1.51±0.2	4
α4L617Aβ2	118±18	4	ND	1±0.07**	5
α4Y309Fβ2	116±19	8	13.88±5	1.52±0.06	4
α4F167Aβ2	142± 15*	5	12.56±4	1.54±0.1	3
α4F167Yβ2	95±9	4	12.71±5	1.51±0.5	3
α4F170Aβ2	86±14	4	11.5±0.5	1.01±0.09**	3
α4F170Iβ2	122±10	4	ND	1.03±0.09**	4
α4I626Aβ2	110±15	4	ND	1.01±0.05**	3
α4I626Fβ2	108±17	4	ND	1.06±0.03**	4
α4F167Y,Y309Fβ2	115±20	5	13.33±18	1.41±0.2	4
α4F170I-I626Fβ2	110±25	5	10.1±18	1.3±0.2	4

FIGURE LEGENDS

Figure 1. Effects of βEST and dFBr on alternate α4β2 nAChRs. A) Structure of 17β-Estradiol (βEST). **B)** Concentration response effects of βEST on the ACh EC_{10} current responses of $(\alpha4\beta2)_2\alpha4$ and $(\alpha4\beta2)_2\beta2$ nAChRs. Data points represent the mean ± SEM of at least 4 experiments. The data were fit to the monophasic Hill equation, as described in Experimental Procedures. The effects of βEST were determined on ACh currents evoked by EC_{10} (3 μM for $(\alpha4\beta2)_2\beta2$) nAChRs and 10 μM for $(\alpha4\beta2)_2\alpha4$ nAChRs. **C)** Structure of desformylflustrabromine (dFBr); **D)** Potentiating effects of dFBr on the ACh responses of alternate $(\alpha4\beta2)_2\alpha4$ and $(\alpha4\beta2)_2\beta2$ nAChRs. The concentration-responses curves were obtained as for those of βEST. Data points represent the mean ± SEM of 5 experiments. For B and D, functional expression of $(\alpha4\beta2)_2\alpha4$ or $(\alpha4\beta2)_2\beta2$ nAChRs was achieved by expressing the concatenated forms of the alternate stoichiometries of the α4β2 nAChRs in *Xenopus* oocytes, as described under Experimental Procedures.

Figure 2. M3 and M4 residues in the α4 nAChR subunit impact dFBr potentiation. A) Full model of $(\alpha4\beta2)_2\alpha4$ with α4 in yellow and β2 in blue on the left and a zoom on the potential dFBr site on the right. Residues that might be involved in binding dFBr are shown as sticks. dFBr is shown in light blue. B) Superimposition of the X-ray structure of $(\alpha4\beta2)_2\beta2$ nAChR onto the homology model used in this study to predict the binding site for dFBr in the α4β2 nAChR. The homology model is shown in yellow and the X-ray structure in grey. Relevant residues are shown as sticks (dark pink in the homology model and grey in the X-ray structure). **C)** Representative current responses elicited by ACh EC_{10} in the absence or presence of dFBr from oocytes expressing mutant α4Y309Aβ2, α4F312Aβ2 or α4L617Aβ2 nAChRs. **D)** Maximal dFBr potentiation of ACh EC_{10} current responses from wild type or mutant $(\alpha4\beta2)_2\alpha4$ or $(\alpha4\beta2)_2\beta2$ nAChRs. The alternate stoichiometries of the α4β2 nAChR were expressed using concatemeric constructs, as described in Experimental Procedures. Maximal potentiation by dFBr of ACh EC_{10} current responses ($I_{max\ pot}$) was calculated as ($I_{ACh\ EC10}$ + dFBr) /$I_{ACh\ EC10}$ from concentration response curve data, as described in Experimental Procedures. Values represent the mean ± SEM of at least 5 independent experiments. Asterisks indicate that the change in $I_{max\ pot.}$ is statistically significant (**, $p < 0.001$, ***, $p < 0.0001$), as measured by one-way ANOVA with Dunnett's correction. Dotted line indicates a potentiation ratio of 1 (no potentiation). The cartoon underlying each column show how many copies of F312A (black dot) are present in the receptors. Red dotted line indicates a potentiation ratio of 1 (no potentiation).

Figure 3. Effects of MTSET on dFBr potentiation of α4β2 nAChRs. A) Representative current traces from α4F617Cβ2 receptors showing potentiation of ACh EC_{10} currents before and after a 2 min application of 1 mM MTSET. **B)** Scatter plot showing changes in dFBr potentiation after MTSET application to wild type or mutant α4β2 nAChRs containing α4L617C or α4F316C subunits. The percentage of change in dFBr potentiation was estimated using the equation: % Change = ((I_{after} /$I_{initial}$) – 1) x 100), where $I_{initial}$ is the response to ACh EC_{10} + dFBr EC_{100} prior to MTSET application and I_{after} is the response to ACh EC_{10} + dFBr EC_{100} after MTSET application. Asterisks indicate values that are significantly different from wild type (*, $p < 0.05$; ***, $p < 0.0001$). **C)** Representative traces showing the rate of MTSET (20 μM) reaction with L617C in the absence or presence of EC_{100} dFBr (10 μM). **D)** For protection assays using α4F617Cβ2 mutant receptors, the observed decreases in dFBr potentiation were plotted versus cumulative MTSET exposure in α4F617Cβ2 receptor. Data obtained from individual assays were normalised to the potentiation measured at t = 0 and fit to a single-exponential decay curve, as described in Experimental Procedures. (●, MTSET alone; ■, MTSET + dFBr). Data points are the means ± SEM from at least three independent assays. Asterisks indicate values that are significantly different from wild type (***, $p < 0.0001$).

Figure 4. Mutations in Cys loop affect dFBr effects on nAChRs. A) Sequence alignment of the agonist-binding-channel gating coupling elements β1-β2 and Cys loop, M3 and M4 transmembrane α-helices and the post-M4 region of nAChR α and β2 subunits. Residues that impact dFBr potentiation in α4β2 nAChRs are highlighted in bold. As shown in the alignment, these residues are conserved in the nAChR family. The post-M4 region is highlighted for all the sequences aligned. Unlike, the residues of the β1-β2, Cys loop and M3, M4 and post-M4 are highly variable in the nAChR family

(1). Sequences were aligned using the T-Coffee sequence alignment tool. **B)** Concentration-response curve for dFBr on wild-type α3β2 nAChRs (●) or α3F310Aβ2 (■) nAChRs. Data points represent the mean ±SEM of at least 4 experiments. The data were fit to the monophasic Hill equation, as described in Experimental Procedures. Inset shows representative ACh current responses traces of wild type or mutant α3β2 nAChRs in the absence or presence of increasing dFBr concentrations (10 μM, 30 μM and 100 μM). **C)** Maximal dFBr potentiation of ACh EC_{10} current from wild type and β1-β2 or Cys loop mutant α4β2 receptors. dFBr potentiation was calculated as (I(ACh EC_{10} + dFBr)/IACh EC_{10}). Dashed line indicates wild type levels of potentiation and dotted line indicates a potentiation ratio of 1 (no potentiation). Asterisks indicate values that are significantly different from wild type (**, $p <$ 0.001).

Figure 5. Post-M4 is a critical determinant of dFBr potentiation. A) Maximal effects of dFBr on wild type and mutant α4β2 nAChRs. Mutations were introduced individually on α4 post-M4. dFBr potentiation was calculated as I(ACh EC_{10} + dFBr)/IACh EC_{10}. Data are the mean ± SEM from at least three oocytes from two or more batches. Dashed line indicates wild type levels of potentiation, whilst the dotted line indicates a potentiation ratio of one (no potentiation). Asterisks indicate values that are significantly different from wild type (**, $p < 0.001$). **B)** Representative traces of the maximal effects of dFBr on α3PPWLAGMIβ2 nAChRs. α3 subunit in wild type receptors has a longer and more hydrophilic post-M4 (LMAREDA). Wild type α3β2 receptors are insensitive to potentiation by dFBr (see Figure 3B). **C)** Concentration-response curves for the effects of dFBr on post-M4 mutants of the α3β2 nAChR. The post-M4 domain of the α3 subunit was changed to that of the α4 subunit, first keeping the α3 PQ motif preceding post-M4 (α3PQWLAGMI) and then substituting PQ for the PP motif found in the α4 subunit (α3PPWLAGMI). F310A effects on the effects of dFBr on α3PPWLAGMIβ2 receptors was also determined. Data were fit by non-linear regression as described in Experimental Procedures.

Figure 6. Cys loop and post M4 interactions affect dFBr potentiation. A) Homology model of α4β2 showing the Cys loop and adjacent M3, M4 and post-M4 regions of a α4 subunit. Note that PP and post-M4 are shown to be helical because the homologous region in the template used (5-HT3 X-ray structure) was found to be helical (36); however, the PP motif most likely disturbs the helicity. Also, note that only the PPWL motif of post-M4 (blue cartoon) is included in the model as the template was missing for the latter four residues of post-M4, the AGMI motif. **B-D).** Representative current responses elicited by ACh EC_{10} traces in the presence and absence of EC_{100} dFBr from α4β2 nAChRs containing the following mutant α4 subunits: α4F170I, α4I626F, α4F170I-I626F **(B)**; α4F167Y, α4L305F, α4F167L-L305F **(C)**; α4F167Y, α4Y309F and β4F167Y-Y309E) α4β2 nAChRs **(D). E)** Histogram of peak EC_{10} ACh currents in the presence of dFBr obtained from oocytes expressing wild type or mutant (α4F170I, α4I626F, α4F170I-I626F, α4F167Y, α4Y309F and β4F167Y-Y309E) α4β2 nAChRs. Data represent the mean ± SEM of at least three independent experiments. Statistical significance was determined by one-way ANOVA with a Dunnett's post-test. *, $p < 0.05$; *** $p < 0.001$. Dashed line indicates wild type level of dFBr potentiation and dotted line indicates a potentiation ratio of 1 (no response).

Figure 7. Cys loop and post-M4 interactions affect βEST potentiation. A and **B)** Representative traces of ACh current responses in the presence and absence of EC_{100} βEST from wild type and mutant receptors. The mutant α4 subunits tested were as follows: **A)** α4F170I, α4I626F, α4F170I-I626F and; **B)** α4F167Y, α4Y309F and β4F167Y-Y309E. **C)** Histogram of peak EC_{10} ACh currents in the presence of EC_{100} βEST obtained from oocytes expressing wild type or mutant (α4F170I, α4I626F, α4F170I-I626F, α4F167Y, α4Y309F and β4F167Y-Y309E) α4β2 nAChRs. Data represent the mean ± SEM of at least three independent experiments. Statistical significance was determined by one-way ANOVA with a Dunnett's post-test. **, $p < 0.001$. Dashed line shows wild type level of βEST potentiation and dotted line indicates a potentiation ratio of one (no potentiation).

Figure 1

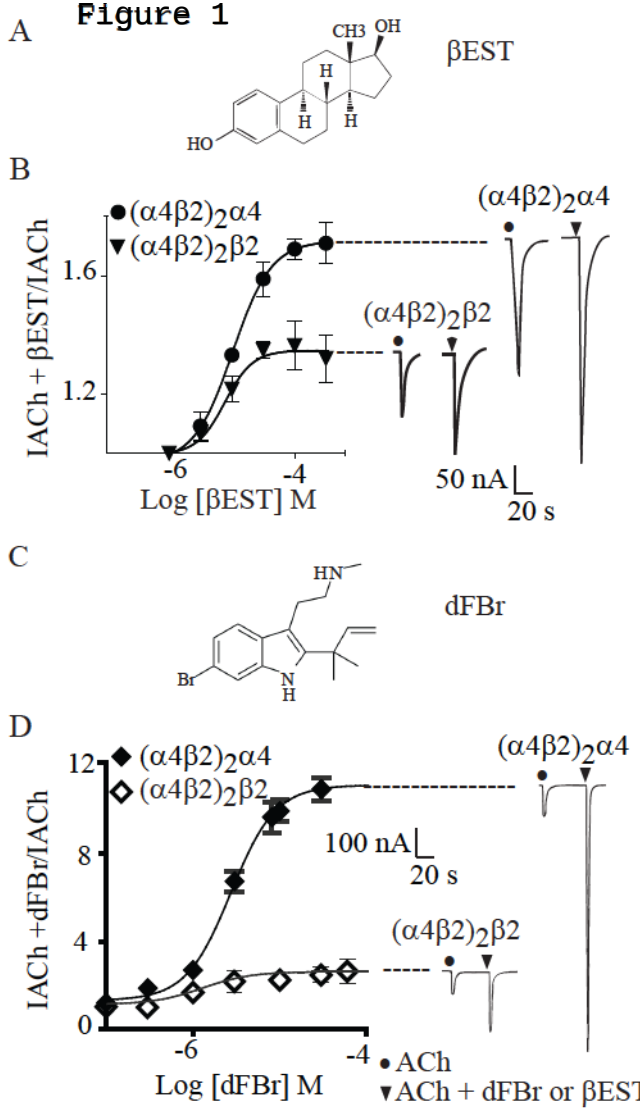
A
CH3
OH
H
H
H
HO
βEST
B
(α4β2)2α4
(α4β2)2β2
IACh + βEST/IACh
1.6
1.2
-6
-4
Log [βEST] M
(α4β2)2α4
(α4β2)2β2
50 nA
20 s
C
HN
Br
N
H
dFBr
D
(α4β2)2α4
(α4β2)2β2
IACh +dFBr/IACh
12
8
4
0
-6
-4
Log [dFBr] M
100 nA
20 s
(α4β2)2α4
(α4β2)2β2
ACh
ACh + dFBr or βEST

Figure 2

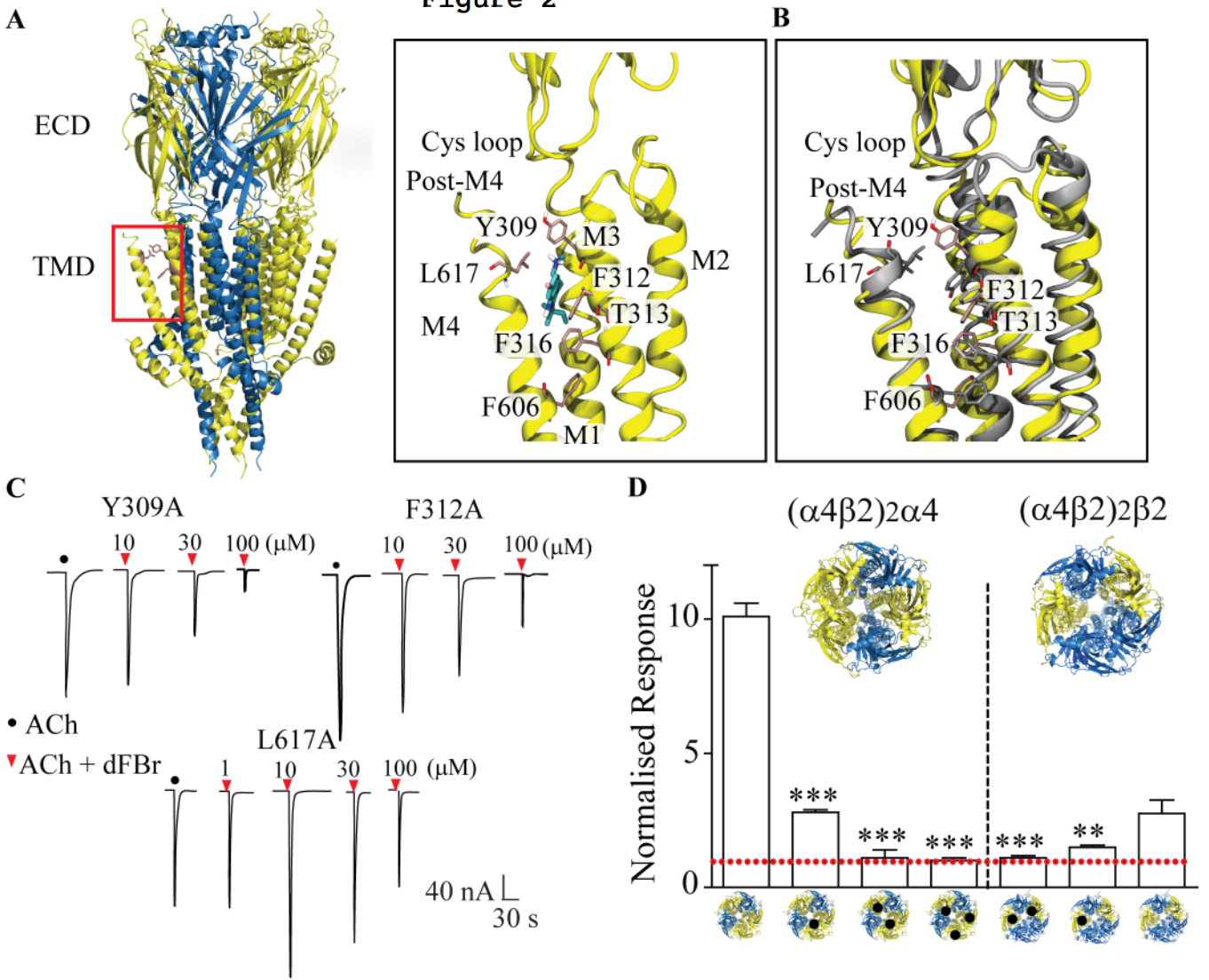
A
ECD
TMD
B
Cys loop
Post-M4
Y309
M3
L617
F312
M2
M4
T313
F316
F606
M1
C
Y309A
F312A
10
30
100 (μM)
• ACh
ACh + dFBr
L617A
1
40 nA
30 s
D
(α4β2)2α4
(α4β2)2β2
Normalised Response
***
**

Figure 3

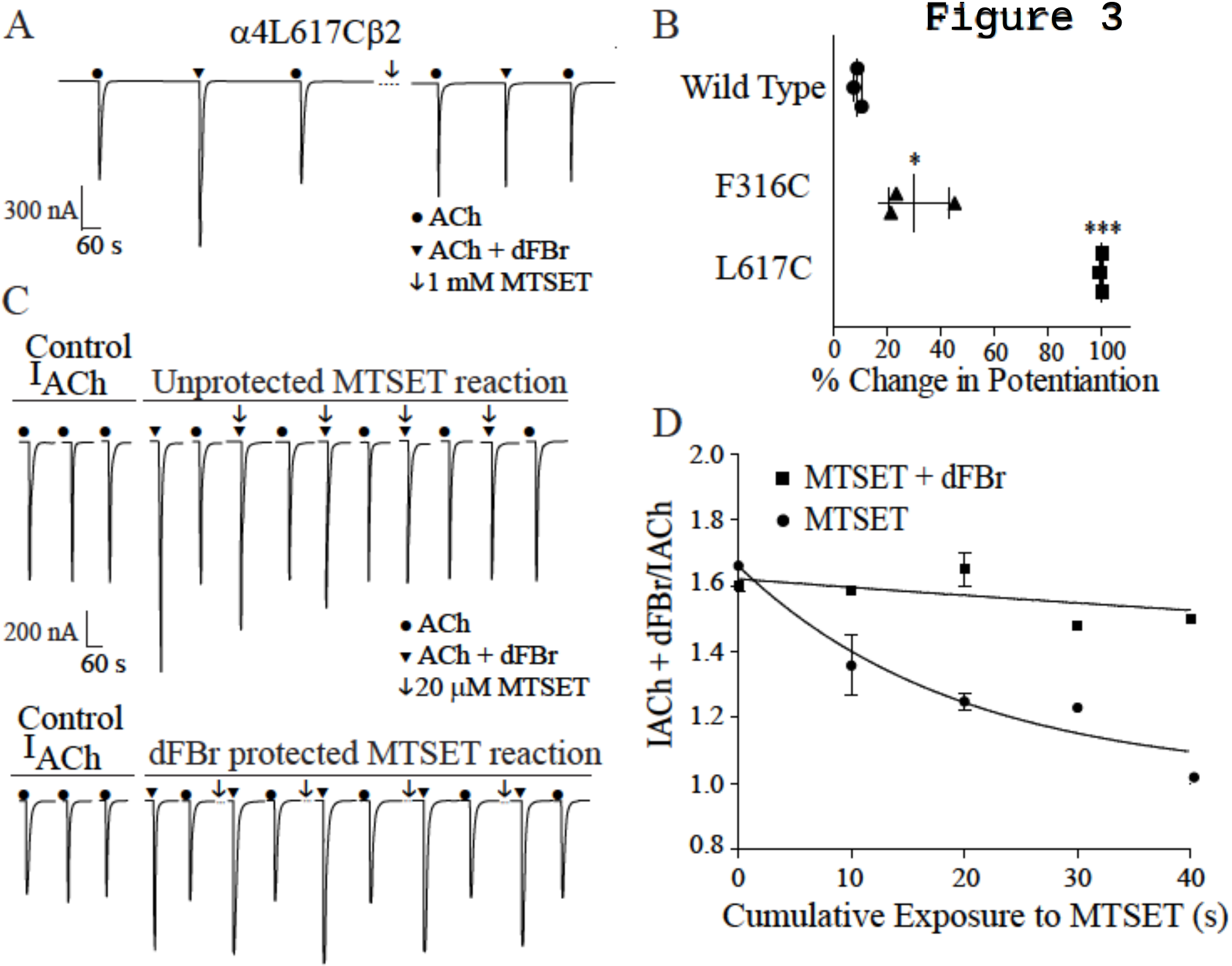
A
α4L617Cβ2
300 nA
60 s
• ACh
▾ ACh + dFBr
↓1 mM MTSET
B
Wild Type
F316C
L617C
*
***
0 20 40 60 80 100
% Change in Potentiantion
C
Control
I ACh
Unprotected MTSET reaction
200 nA
60 s
• ACh
▾ ACh + dFBr
↓20 μM MTSET
Control
I ACh
dFBr protected MTSET reaction
D
MTSET + dFBr
MTSET
IACh + dFBr/IACh
2.0
1.8
1.6
1.4
1.2
1.0
0.8
0 10 20 30 40
Cumulative Exposure to MTSET (s)

Figure 4

A

		β1-β2 loop		β6-β7 loop
α4	(75)	DVDEKNQMMTTN	(158)	KSSCSIDVTFFPFDQQNCTM
α2	(97)	DVDEKNQMMTTN	(180)	KSSCSIDVTFFPFDQQNCKM
α3	(73)	KVDEVNQIMETN	(156)	KSSCKIDVTYFPFDYQNCTM
α1	(62)	NVDEVNQIVTTN	(169)	KSYCEIIVTHFPFDEQNCSM
α7	(64)	DVDEKNQVLTTN	(147)	KSSCYIDVRWFPFDVQHCKL
β2	(69)	SVHEREQIMTTN	(152)	KSACKIEVKHFPFDQQNCTM

		M3		M4	Post-M4
α4	(309)	YLLFTMIFVTLSIVITVFVLNV	(601)	IFLWMFIIVCLLGTVGLFLP	P—WLAGMI----------
α2	(331)	YLLFTMIFVTLSIVITVFVLNV	(503)	IFLWLFIIVCFLGTIGLFLP	P—FLAGMI----------
α3	(307)	YLLFTMIFVTLSIVITVFVLNV	(478)	IFLWVFTLVCILGTAGLFLQ	P—LMAREDA----------
α1	(322)	YMLFTMVFVIASIIITVIVI	(454)	ILLGVFMLVCIIGTLAVFAGR	—LIELNQQG----------
α7	(296)	YFASTMIIVGLSVVVTVIVLQY	(470)	LCLMAFSVFTIICTIGILMSAPNFVEAVSKDFA----------	
β2	(300)	GKYLMFTMVLVTFSIVTSVCVLNV	(459)	DRLFLWIFVFVCVFGTIGMF	PLFQNYTTTTFLHSDHSAPSSK

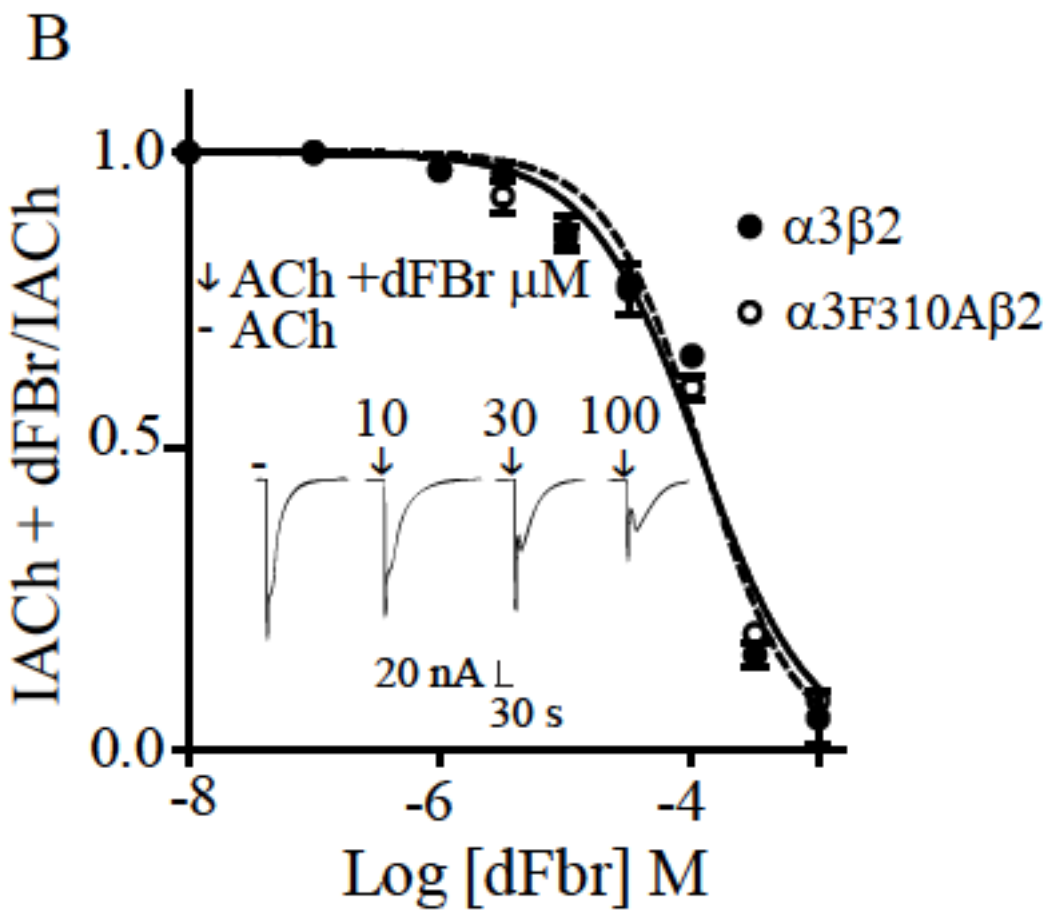

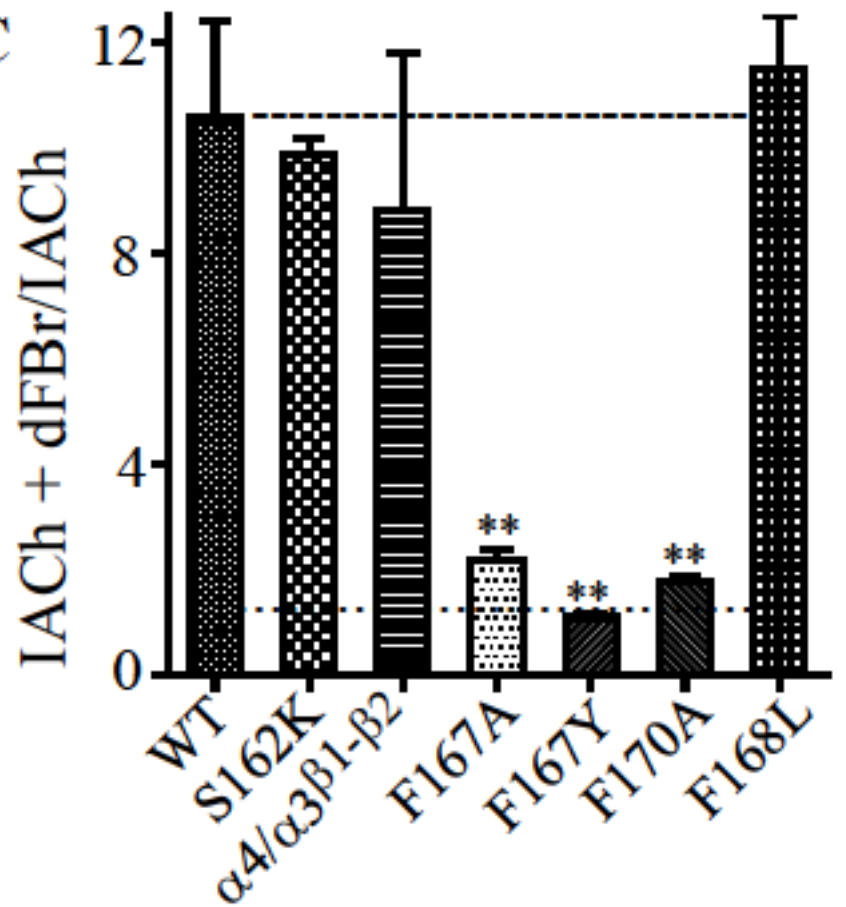

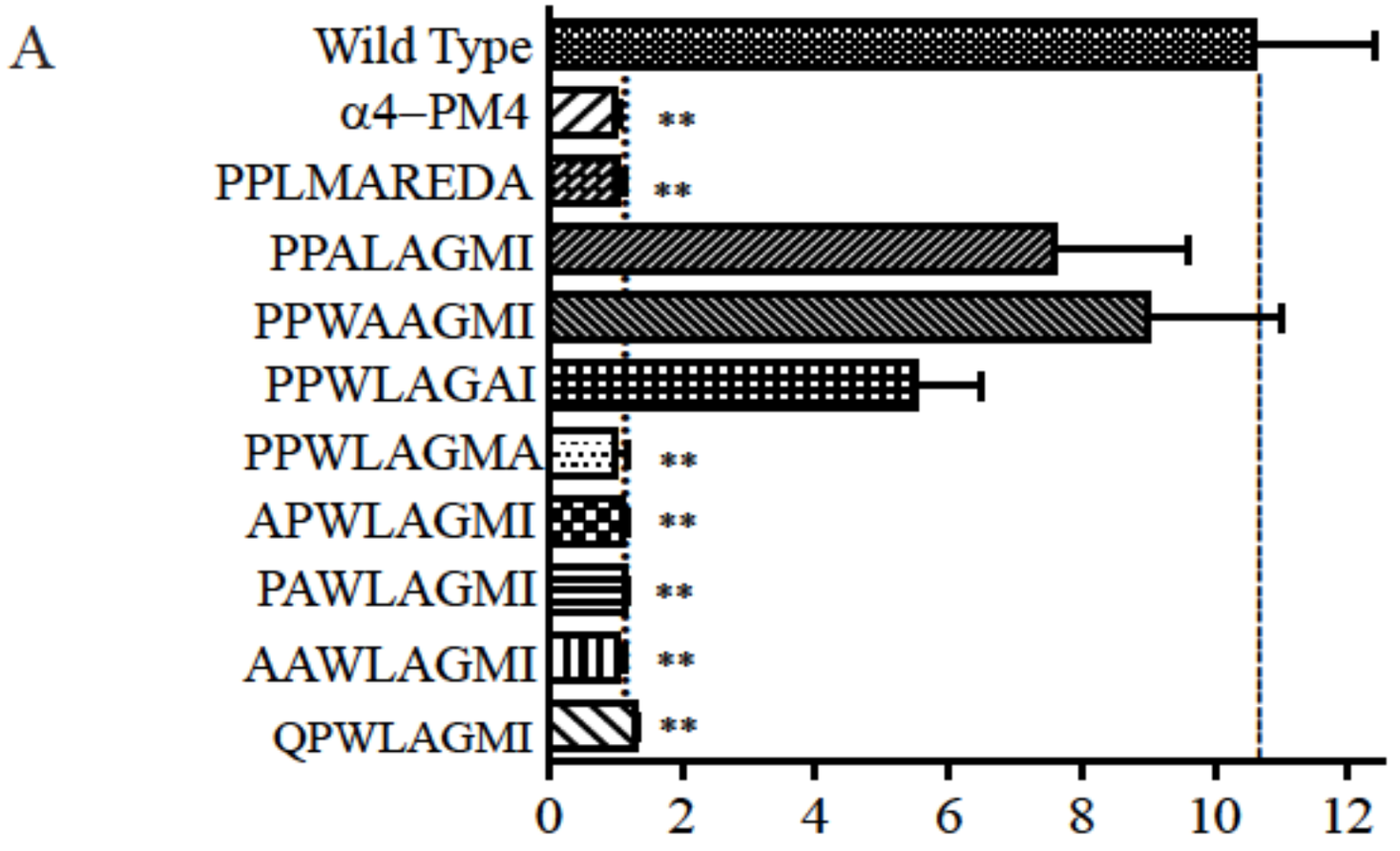
A
Wild Type
α4–PM4
PPLMAREDA
PPALAGMI
PPWAAGMI
PPWLAGAI
PPWLAGMA
APWLAGMI
PAWLAGMI
AAWLAGMI
QPWLAGMI
**
0
2
4
6
8
10
12

Figure 5

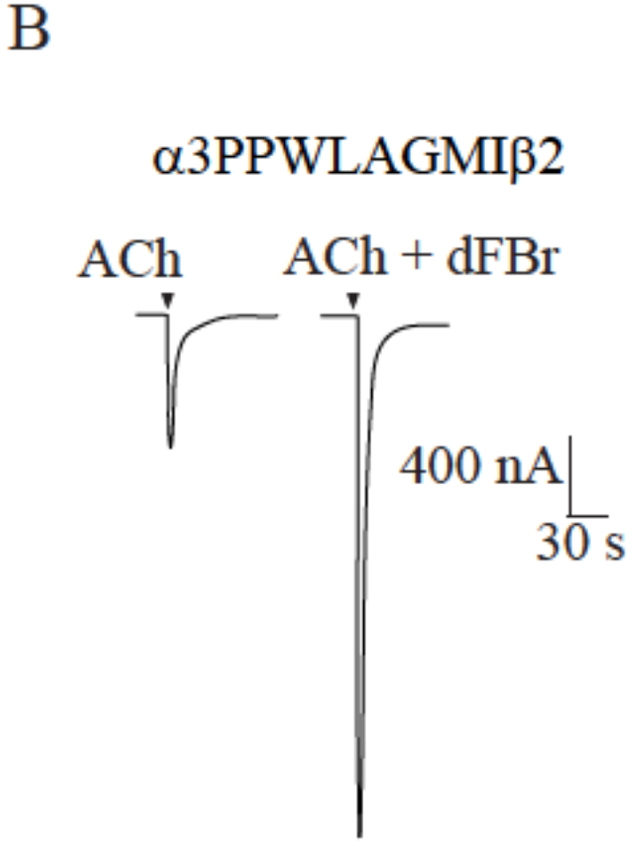
B
α3PPWLAGMIβ2
ACh
ACh + dFBr
400 nA
30 s

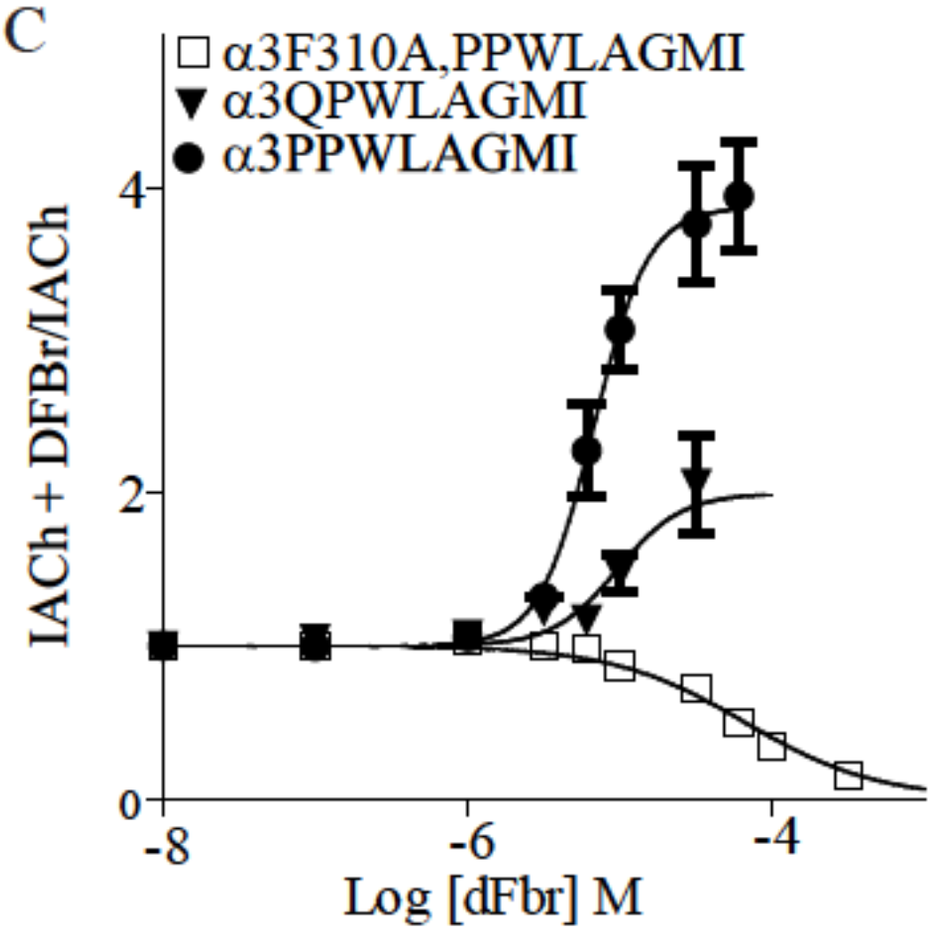
C
α3F310A,PPWLAGMI
α3QPWLAGMI
α3PPWLAGMI
IACh + DFBr/IACh
0
2
4
-8
-6
-4
Log [dFbr] M

Figure 6

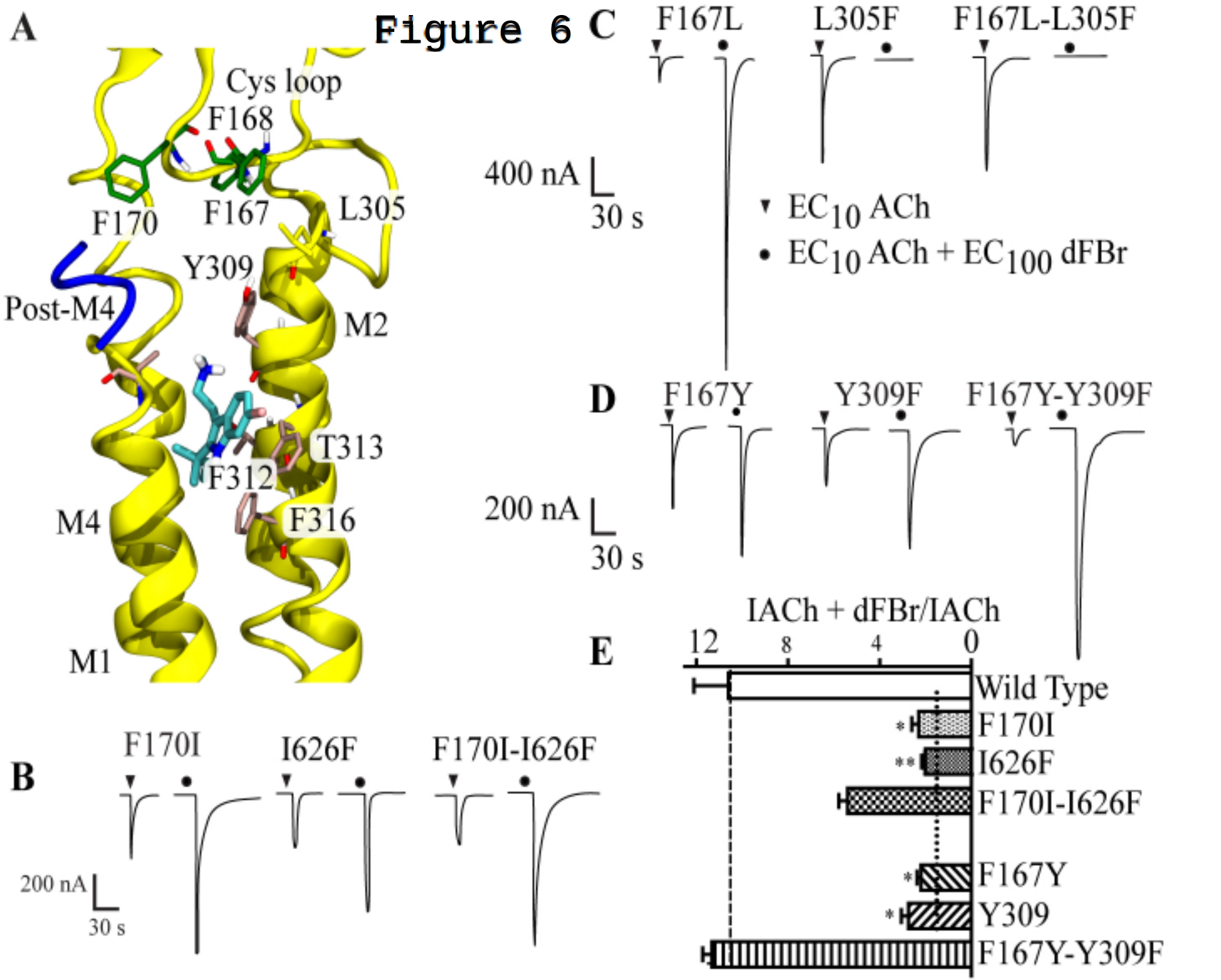
A
Cys loop
F168
F170
F167
L305
Y309
Post-M4
M2
T313
F312
M4
F316
M1
B
F170I
I626F
F170I-I626F
200 nA
30 s
C
F167L
L305F
F167L-L305F
400 nA
30 s
EC10 ACh
EC10 ACh + EC100 dFBr
D
F167Y
Y309F
F167Y-Y309F
200 nA
30 s
E
IACh + dFBr/IACh
12
8
4
0
Wild Type
F170I
I626F
F170I-I626F
F167Y
Y309
F167Y-Y309F

Figure 7

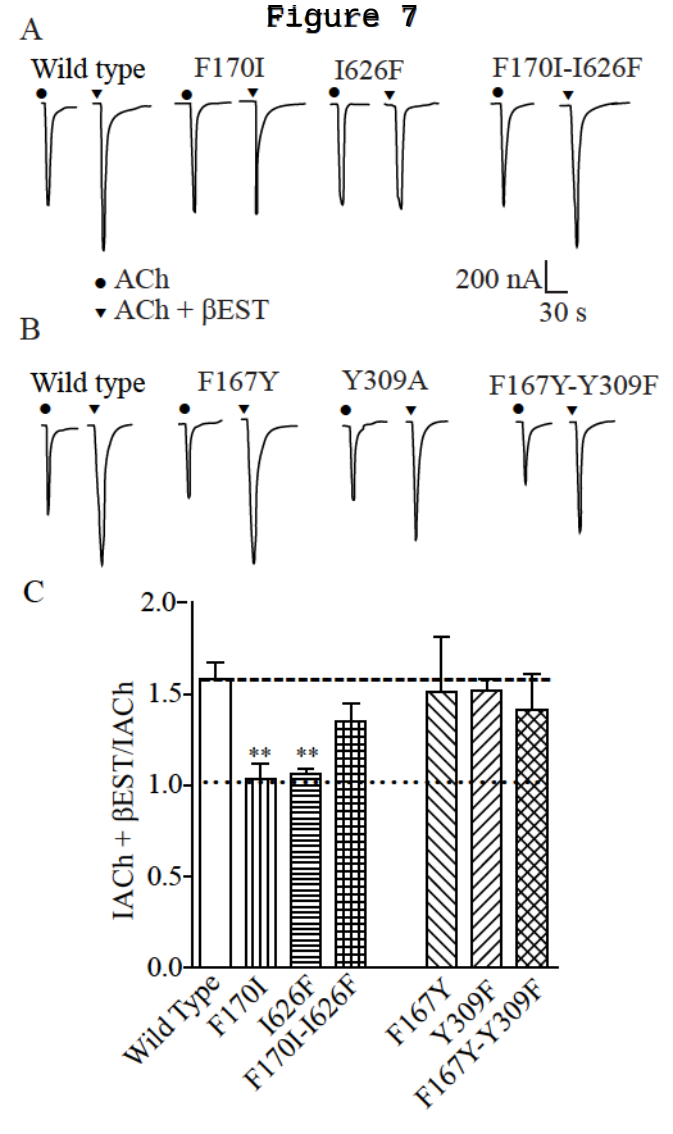
A
Wild type
F170I
I626F
F170I-I626F
ACh
ACh + βEST
200 nA
30 s
B
Wild type
F167Y
Y309A
F167Y-Y309F
C
IACh + βEST/IACh
2.0
1.5
1.0
0.5
0.0
**
**
Wild Type
F170I
I626F
F170I-I626F
F167Y
Y309F
F167Y-Y309F